Sn-M (M=Sn, Bi, In) Bimetallic Catalysts for Electrocatalytic Conversion of CO_2 to Formic Acid

Master Thesis
Conducted at the

Group of Molecular and Materials Chemistry
Institute of Materials Chemistry
Vienna University of Technology

By
Dorottya Varga, BSc.
Under supervision by
Univ.Prof. Mag.rer.nat. Dr.rer.nat.
Dominik Eder
and
Univ. Ass. Dr. Rer. Nat. Doğukan H. Apaydın

Table of contents

1. Abstract

Carbon dioxide is a gas found in the atmosphere, produced primarily through natural processes such as the respiration of plants and animals, the decomposition of organic matter, and the breakdown of living organisms. However, the natural carbon cycle has been significantly disrupted by anthropogenic CO_2 emissions, contributing to climate change. To mitigate the impact of elevated CO_2 levels, efforts have been made to develop an artificial carbon cycle that captures atmospheric as well as anthropogenic CO_2 and converts it into value-added chemicals. Among these, liquid organic hydrogen storage materials have gained attention for their ease of handling and potential to store and release hydrogen (on demand)efficiently.

Formic acid has emerged as a promising candidate for this purpose due to its ability to act as a hydrogen carrier under mild conditions. One of the most effective yet challenging methods to convert CO_2 into formic acid is through electrochemical reduction. This process requires highly selective and stable catalysts, and recent research has highlighted the efficiency of Sn-based bimetallic alloys for this application. Metals such as Sn, In, and Bi, which belong to the p-block of the periodic table, have shown the ability to selectively produce formate through the electrochemical reduction of CO_2. By combining two of these metals, it is possible to enhance their catalytic performance, leading to increased production rate of the desired product.

This study focuses on the development of Sn-based bimetallic alloy electrodes through straightforward preparation methods such as electrodeposition and dropcasting of a secondary metal-oxide ink onto a Sn substrate. The prepared electrodes were characterized using X-ray diffraction (XRD), linear sweep voltammetry (LSV), and cyclic voltammetry (CV). The catalytic performance of all electrodes was evaluated, and the results indicate that bimetallic alloys exhibit significantly higher Faradaic efficiency (FE) at lower overpotentials compared to bulk Sn electrodes. Moreover, the dropcasting method demonstrated greater reproducibility in electrode preparation, further enhancing the overall performance in formic acid production.

1.1. Kurzfassung

Kohlendioxid ist ein in der Atmosphäre vorkommendes Gas, das hauptsächlich durch natürliche Prozesse wie die Atmung von Pflanzen und Tieren, die Zersetzung organischer Stoffe und den Abbau lebender Organismen entsteht. Der natürliche Kohlenstoffkreislauf ist jedoch durch die anthropogenen CO2-Emissionen erheblich gestört worden, was zum Klimawandel beiträgt. Um die Auswirkungen des erhöhten CO2-Gehalts zu verringern, wurden Maßnahmen zur Entwicklung eines künstlichen Kohlenstoffkreislaufs entwickelt, der sowohl atmosphärisches als auch anthropogenes CO2 auffängt und in hochwertigen Chemikalien umwandelt. Dabei haben flüssige organische Wasserstoffspeichermaterialien aufgrund ihrer einfachen Handhabung und ihres Potenzials, Wasserstoff effizient zu speichern und (bei Bedarf) freizusetzen, große Aufmerksamkeit gewonnen.

Ameisensäure hat sich als hoffnungsvoller Kandidat für diesen Zweck erwiesen, da sie unter milden Bedingungen als Wasserstoffträger fungieren kann. Eine der effektivsten, aber auch schwierigsten Methoden zur Umwandlung von CO2 in Ameisensäure ist die elektrochemische Reduktion. Dieser Prozess erfordert hochselektive und stabile Katalysatoren, und die neuere Forschung hat die Effizienz von Bimetalllegierungen auf Sn-Basis für diese Anwendung hervorgehoben. Metalle wie Sn, In und Bi, die zum p-Block des Periodensystems gehören, haben die Fähigkeit bewiesen, durch elektrochemische Reduktion von CO2 selektiv Formiat zu erzeugen. Durch die Kombination von zwei dieser Metalle kann ihre katalytische Leistung verbessert werden, was zu einer höheren Produktionsrate des gewünschten Produkts führt.

Diese Studie konzentriert sich auf die Entwicklung von Elektroden aus einer Bimetalllegierung auf Sn-Basis durch einfache Präparationsmethoden wie die Elektroabscheidung und das Dropcasting einer sekundären Metalloxid-Ink auf ein Sn-Substrat. Die hergestellten Elektroden wurden mittels Röntgenbeugung (XRD), linearer Voltammetrie (LSV) und zyklischer Voltammetrie (CV) charakterisiert. Die katalytische Leistung aller Elektroden wurde bewertet, und die Ergebnisse weisen darauf hin, dass die bimetallischen Legierungen im Vergleich zu reinen Sn-Elektroden bei niedrigeren Überspannungen eine deutlich höhere Faradaische Effizienz (FE) aufweisen. Darüber hinaus zeigte die Dropcasting-Methode eine größere Reproduzierbarkeit bei der Elektrodenherstellung, was die Gesamtleistung bei der Herstellung von Ameisensäure weiter verbesserte.

2. Introduction

The rise in atmospheric CO_2 levels as a result of human activities is a growing concern due to its negative impacts on the environment and climate. CO_2 is a greenhouse gas, which means that it traps heat in the Earth's atmosphere, leading to global warming and climate change. As CO_2 levels continue to rise due to human activities like burning fossil fuels, deforestation, and agriculture, the planet's temperature increases, leading to more frequent and severe weather events, rising sea levels, and melting glaciers and ice caps. Additionally, increased CO_2 levels can also have indirect effects on the environment, such as ocean acidification, which can harm marine life and disrupt ecosystems. It is essential to reduce CO_2 emissions and take action to mitigate the effects of climate change before irreversible damage is done to the planet. To combat this issue, the conversion of CO_2 into useful products, such as formic acid and syngas has emerged as a promising approach.

Formic acid is a versatile chemical that can serve as a renewable energy carrier, a platform chemical for various industries, and a means for CO_2 capture and utilization. Electrochemical reduction of CO_2 to formic acid is a promising technique because it offers high selectivity and tunability over the reaction. Additionally, the process can be powered by renewable energy sources such as solar and wind, making it a sustainable way to mitigate CO_2 emissions. Thus, CO_2 reduction to formic acid has the potential to provide a solution to both reducing atmospheric CO_2 levels and creating a sustainable source of energy in the form of indirect source of hydrogen.

Hydrogen can be used as a fuel in combustion engines, either alone or in combination with other fuels like natural gas. In this case, hydrogen is burned in the engine to produce energy, and the byproduct is water vapor.

Formic acid is a stable liquid that can be stored and transported without the need for high-pressure tanks or complex infrastructure. It also has a high energy density, meaning that a relatively small volume of formic acid can store a large amount of energy. For comparison, commercially available fuel options, such as gasoline, biodiesel and diesel offer an energy density in the range of 9.17 to 9.61 kWh/L[39], while a high pressure (700bar) on-board hydrogen storage due to greater energy losses only 1.4 kWh/L, while having 5.7 wt% H_2-content. Formic acid, on the other hand, contains 4.4 wt% hydrogen, which is equivalent to 1.77 kWh/L energy density[8].

The focus of this thesis project is to utilize p-block metals, such as Sn, In and Bi for electroreduction of CO_2 to formic acid.
Due to the high overpotential for H_2 evolution reaction (HER) of these metals, they are considered as efficient catalyst to reduce CO_2.The large overpotentials to drive CO_2 reduction tends to result in highly reactive intermediates and 2, 4, 8 and 12 electron transfer reactions, that produce a bigger variety of products (CO, formate, methane, methanol, ethylene). According to the study of Hori[11] the p-block metals and their oxides have displayed high selectivity towards formate and formic acid production.

There are 2 known pathways of p-block metals to formic acid production, one via direct carbon bond with $COOH^*$ intermediate from stabilized CO_2^*-radicals, and the second path is through a coupled proton-electron transfer via $OCHO^*$- intermediate. It is believed that bimetallic catalysts can increase the efficiency (selectivity) of CO_2RR by stabilizing one OCHO* intermediate [2], [3]. Hence this thesis focuses on the effect of different bimetallic catalysts on the reaction performance.

3. Motivation

The increasing concentration of atmospheric CO_2 due to human activities poses a significant challenge to environmental sustainability and climate stability. The adverse effects of excessive CO_2 emissions, including global warming, extreme weather events, and ocean acidification, necessitate immediate and effective mitigation strategies. While various approaches have been explored to reduce atmospheric CO_2 levels, the electrochemical reduction of CO_2 into valuable chemicals presents a promising and sustainable solution.

Among the various CO_2-derived products, formic acid has garnered substantial interest due to its versatility as a hydrogen carrier, energy storage medium, and feedstock for industrial applications. Its ability to store and release hydrogen under mild conditions makes it a viable candidate for clean energy technologies, providing an alternative to traditional hydrogen storage methods that require high-pressure systems. The potential of formic acid to facilitate a sustainable energy transition further underscores the importance of developing efficient and selective catalysts for CO_2 reduction.

To achieve high selectivity and efficiency in electrochemical CO_2 reduction, catalysts play a critical role. Recent studies have demonstrated that p-block metals, particularly Sn, In, and Bi, exhibit high selectivity for formate production. By leveraging the synergistic effects of bimetallic alloys, catalytic performance can be enhanced, leading to improved Faradaic efficiency and reduced overpotentials. However, the challenge remains in optimizing the composition and preparation methods to achieve reproducible and scalable electrode materials.

This thesis aims to address these challenges by investigating Sn-based bimetallic alloys for the electroreduction of CO_2 to formic acid. Through electrodeposition and dropcasting techniques, the study seeks to develop and characterize efficient catalysts with enhanced stability and selectivity. By systematically analyzing the impact of alloy composition and preparation methods on catalytic performance, this research contributes to the ongoing efforts in developing viable CO_2 utilization strategies. Ultimately, this work aligns with the broader goal of mitigating climate change by integrating renewable energy sources into carbon-neutral chemical production processes.

4. Theoretical Background

This chapter aims to provide an overview on how bimetallic catalysts work, explanation to electrocatalytic CO_2 reduction reaction and formic acid as a mean of hydrogen source for sustainable fuel production.

4.1. Formic acid

Formic acid, with the chemical formula HCOOH, is a simple organic compound belonging to the carboxylic acid family. It is a colorless liquid with a pungent odor and is miscible with water and most organic solvents. Formic acid is naturally found in various organisms, including ants, where it serves as a defense mechanism and is responsible for their characteristic acidic bite.

Formic acid holds significant importance across a wide range of industries due to its versatile properties and diverse applications. One of its primary uses is as a preservative and antibacterial agent in animal feed and silage, where it helps inhibit the growth of mold and bacteria, thereby extending shelf life and maintaining quality. Additionally, formic acid is employed as a pH regulator and acidifier in various industrial processes, such as textile and leather manufacturing, where it facilitates dyeing, tanning, and finishing operations.

Moreover, formic acid plays a crucial role in the production of a variety of chemicals and materials. It serves as a precursor in the synthesis of various pharmaceuticals, agrochemicals, and fine chemicals, contributing to the pharmaceutical and chemical industries. Furthermore, formic acid is utilized as a key intermediate in the manufacture of other important compounds, including formate salts, formaldehyde, and methanol, which are integral to numerous industrial processes.

In recent years, formic acid has garnered increasing attention as a potential renewable energy carrier and chemical feedstock in the context of sustainable development and green chemistry. Its ability to store and release hydrogen under mild conditions makes it an attractive candidate for hydrogen storage and transportation, offering potential solutions to challenges associated with hydrogen economy and renewable energy integration. Nonetheless formic acid is also relatively nontoxic and noncorrosive, which enables easy handling of the substance. Formic acid contains 4,4 wt% hydrogen[4],[8] which approaches the desired 5,5 wt% content to be an efficient hydrogen storage material according to the DOE. A 1L hydrogen gas container can hold up to 9.8 mol of the element at high pressures while 1L of formic acid can put out 26.5 mol of hydrogen, and the liquid storage does not require high pressures and such careful handling necessary with the gaseous hydrogen container[4].

4.1.1. Formic acid production

In the past formic acid was mainly produced from biomass-based precursors, such as tartaric acid (Döbereiner), sugar, starch, rye and maze. These feedstocks were hydrolized by sulfuric

acid and depending on the type of precursor the yield varied. There are also records of formic acid winning through the distillation of ants which gives the German name of the acid Ameisensaure.

Significant increase of the yield was found when the solution of biomass-derived sugars with the addition of potassium dichromate was distilled with slow addition of sulfuric acid.
Further developments of formate synthesis also involved oxalic acid as a starting material which was decomposed in the presence of sulfuric acid.

In later years the synthesis of potassium formate from CO and wet potash enabled an effective way to obtain formic acid by treating the alkali formate with sulfuric acid and then separate the carboxylic acid through distillation.

$$KOH + CO \rightarrow HCOOK$$

This acidolysis method is still frequently used in the industry, as potassium-, sodium- and calcium formates are abundantly available due it being a side product of polyhydric alcohol production.

$$2HCOONa + H_2SO_4 \rightarrow 2HCOOH + Na_2SO_4$$

Or

$$(HCOO)_2Ca + H_2SO_4 \rightarrow 2HCOOH + CaSO_4$$

A downside of this synthesis pathway is the production of sulfate salts, which in contrast does not occur in the case of methyl formate hydrolysis. This process is predominantly used to obtain formic acid industrially.

The cabonylation of methanol proceeds at 80 °C temperature and 4.5 MPa pressure, with the addition of 2.5 wt% sodium methoxide catalyst. Under these conditions the conversion of CO is at 95% rate while the methanol is much lower, however unconverted methanol is always being recycled during the process.
Important factors for successful synthesis are the pureness of the CO source, as substantial amount of CO_2 can cause the catalyst to precipitate as carbonate. Furthermore, the catalyst undergoes a side reaction with methyl formate creating formate salts, which can result again in precipitation and blockage in the acid plant.
Lastly the sodium methoxide also promotes the reverse reaction when heated causing the decomposition of methylformate, therefore the catalyst must be neutralized once the carbonylation process has ended.

After obtaining methyl formate a hydrolysis steps follows, this can be done with the presence of high excess water and autocatalysis, as formic acid itself can act as a catalyst in the reaction. Kemira-Leonard process utilizes the autocatalysis method for the hydrolysis, while the BASF Process relies more on a 5:1 molar ratio of water and methyl formate and the excess water is then extracted with a secondary amide.

A third variant of this synthesis pathway is originating from the Soviet Union, where the hydrolysis is carried out in a two-zone column, separated by a fixed bed acidic ion-exchange resin. The upper part is filled with water, while the lower part is fed with methyl formate at 100-107 °C. Hydrolysis takes place in both zones of the column, in the water phase the ion exchange resin acts as a catalyst, while in the lower zone the aforementioned autocatalysis takes place, til the two phases are completely exchanged. Methanol and methyl formate is then removed from the upper zone while formic acid and water from the bottom.

Other processes involve sustainable solutions such as using biomass as precursors instead of fossil feedstocks. Biomass based precursors often undergo acidolysis, wet-oxidation and catalytic oxidation. Amongst the feedstocks reportedly sugars such and glucose (755%) and saccharides (85%), and glycerol (94-99%) serves as precursors with the highest yields for formic acid production. Glycerol has been also an attractive candidate for this purpose due its lowered prices as it is readily being produced in higher quantities for biodiesel usage.
Sugars and carbohydrates are easily converted to formic acid via hydrothermal oxidation with excess hydrogen peroxide in the presence of sodium hydroxide at mild temperatures. While converting glycerol to formic acid can be achieved using iron (III)-salts and hydrogen peroxide as oxidative agent. This process can take place even at room temperature and in aqueous medium.

Lastly, formic acid can be obtained from carbon dioxide as a starting material. One way is the hydrogenation of the precursor in alcohol which provides a water-free environment, offering a simpler product recovery.
Another way utilizing CO_2 to formic acid conversion is through electrochemical processes. These efforts provide heterogenous catalysis and even milder reaction conditions towards formate, making this way of production highly sustainable, while also providing reduced carbon dioxide emission.
The heterogenous system also enables simplified product purification processes.

4.1.2. Formic acid to hydrogen fuel

Oxidation of formic acid can occur in two different ways, dehydration giving CO and water and dehydrogenation resulting in CO_2 and H_2. These two groups of products can be converted into each other using the water-gas shift procedure at high temperatures.

$$HCOOH \rightarrow CO + H_2O(dehydration)$$

$$\downarrow\uparrow Water - Gasshift$$

$$HCOOH \rightarrow CO_2 + H_2(dehydrogenation)$$

Using formic acid in solid oxide fuel cells brings us to the conclusion that the dehydration pathway is undesired, because the produced CO acts as a poison to most catalysts. The dehydrogenation process also supplies with CO_2 that can be recycled for further formic acid production, which results in a closed carbon cycle with little to no emission.

4.1.3. Storage and transportation

Since this thesis aims to provide means to create easier ways to transport and store hydrogen as fuel. It is important to clarify that while hydrogen is a gaseous element and in general it is more difficult to handle its containers due to the high pressures and the temperature regulations. Formic acid also has its hurdles when it comes to transportation and storage, especially when it comes to highly concentrated formic acid, as it can decompose into toxic CO and H_2O in liquid phase. Formic acid containers with concentrations of 99wt% or more should not be transported or stored in closed vessels, and the storage units must be well ventilated. Due to the corrosive properties of the acid the containers are also regulated to one specific type of austenitic steel (CrNi steel, AISI 316). For laboratory use quantities glass and polyethylene vessels are also appropriate.

4.2. Electrocatalytic CO_2-reduction

Electrocatalytic reduction of carbon dioxide to value added chemicals aims to provide a solution to environmental problems arising from the increased emission of CO_2 and to the energy crisis caused by the consumption of fossil fuel resources. Carbon dioxide is a highly stable molecule with linear centrosymmetric structure and double bonds between the carbon and oxygen atoms. CO_2 conversion electrochemically is an energetically uphill process requiring large overpotentials. This is mainly caused by the rate limiting kinetics of the intermediate-formation and its stabilization on the catalyst surface. The first electron -transfer to create $CO2^{\bullet-}$ radical intermediate is highly unfavourable (-1.9V vs. SHE in aqueous medium) [2], [30], thus efforts have been made to avoid the formation of this intermediate through proton-assisted multiple-electron transfer to reduce carbon dioxide and lower the energy barriers. The co-existence of multiple proton-coupled electron transfer reaction pathways can lead to numerous products, the half-reactions and their formal potentials ($E^{0'}$) are listed in the Table 1. This table also contain the competing reaction, hydrogen evolution reaction (HER), that is always present along with the electrochemical reduction of CO_2, this process is unavoidable since the catalytic strategy is to employ proton assisted electron-transfer pathway for CO_2RR.

Table 1 List of possible half-reactions in electrochemical carbon dioxide reduction[2]

CO_2RR half-reactions	***$E^{0'}$ [V] vs SHE at pH 7***
$CO_2 + e^- \rightarrow CO_2^-$	-1.9
$CO_2 + 2e^- + 2H^+ \rightarrow HCOOH\ (l)$	-0.61
$CO_2 + 2e^- + 2H^+ \rightarrow CO\ (g) + H_2O$	-0.53
$CO_2 + 4e^- + 4H^+ \rightarrow HCHO\ (l) + H_2O$	-0.48
$CO_2 + 6e^- + 6H^+ \rightarrow CH_3OH\ (l) + H_2O$	-0.38
$CO_2 + 8e^- + 8H^+ \rightarrow CH_4\ (g) + 2H_2O$	-0.24
$2CO_2 + 12e^- + 12H^+ \rightarrow C_2H_4\ (g) + 4H_2O$	-0.34

$2e^- + 2H^+ \rightarrow H_2\ (g)$	-0.42

Furthermore, it becomes evident that thermodynamically it should be more favourable to convert carbon dioxide into alcohols and other hydrocarbon products based on the relationship:

$$\Delta G = -nFE^0$$

where n is the number of transferred electrons during the redox reaction, F is the Faraday constant and E^0 is the standard reduction potential. The more positive this standard potential is the more likely the reaction will go forth, hence based only on these values the above-mentioned products should be more likely to form in the electrochemical reduction of carbon dioxide.

On the other hand, the reaction is also heavily influenced by the kinetics. Electron transfer at catalytic sites will more likely happen where the hydrogen concentration is more abundant, furthermore the hydrogenation of adsorbed C_1 intermediates is kinetically easier than the formation of C-C bond [2]. Since the catalytic sites for the electroreduction of CO_2 are located on the electrode surface this reaction can be regarded as a heterogeneous catalysis, where the working electrode is the catalyst and the reactants are present in the electrolyte and the electron exchange takes place at the electrode-electrolyte interface. In contrast to homogeneous catalysts where the molecules are dissolved in the electrolyte and the catalyst acts as a redox shuttle between electrode and carbon dioxide[2].

Through potentiostatic control negative charge on the cathode (working electrode) surface is created which results in strong interaction between reactants in the electrolyte solution and the working electrode surface, called the electrical double layer. This double layer consists of an array of charged species and/ oriented dipoles[12]. The structure of this electrical double layer influences the reduction of carbon dioxide since the adsorption and the bond rearrangement of the intermediates occurs within the Helmholtz-layer, which is a part of this aforementioned domain.

This process occurs in the following steps: Chemical adsorption as mentioned previously, this step is heavily influenced by the concentration of carbon dioxide in the electrolyte. In the next step electron transfer takes place, this can be counteracted or paired up with proton migration between the catalyst and the reactant, which results in breaking either the C-O bond and/ or forming the C-H bond. This step is considered to be the bottleneck of the reaction for the formerly explained reasons in this section, while discussing the kinetics of it. And lastly, the product desorption from the catalyst surface and diffusion into the electrolyte. In Figure 1. depicted are several mechanistic models of this process to form formic acid with heterogeneous electrochemical reduction of carbon dioxide.

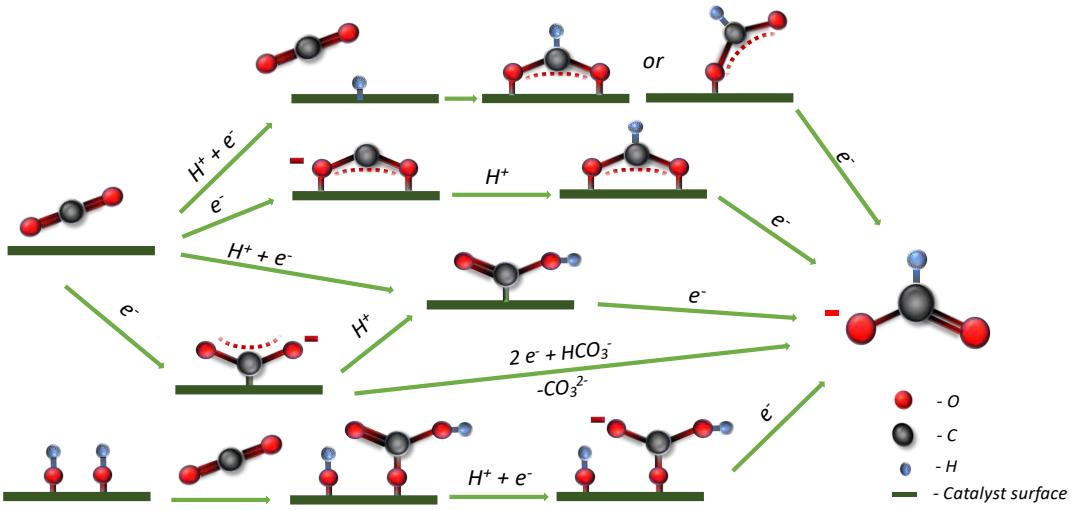

Figure 1 Possible reaction mechanisms of carbon dioxide reduction to formate

On the top there are two pathways which involve a monodentate or bidentate intermediate adsorbed to the catalyst surface via one or two oxygen atoms (OCHO-intermediate). The difference between the two mechanisms is that in the case of the first reaction carbon dioxide is being inserted into a metal-hydrogen bond on the catalyst surface, while in the case of the second reaction it is a direct protonation of the intermediate, the proton is supplied by the electrolyte.

In the lower section of the scheme an alternative mechanism is presented in which the $CO2^{\bullet-}$ radical reacts with a proton nearby to form $HCOO^-$, this process was found to be enhanced in the presence of HCO_3^- [30] in electrocatalytic reduction of carbon dioxide on Sn-based catalysts. In this case the electron transfer and the $CO2^{\bullet-}$ adsorption is followed by a proton transfer from HCO_3^-. The proton transfer then lastly can trigger an additional electron transfer from the electrode to the adsorbed species resulting in formate [18]. This reaction pathway may also result in CO formation. Lastly, on the bottom of the scheme is a pathway found to be taking place with tin oxide electrodes, through reduction of the SnO_2 on the surface first forms a Sn-oxyhydroxyde layer[20], which then reacts with carbon dioxide. In the following steps two electron and a proton is being transferred to the surface bound carbonate to form formate upon desorption, which in result also recovers the oxyhydroxyde. This reaction pathway is also known as surface-bound carbonate intermediate route.

4.3. Catalysts

4.3.1. Bulk metals

The catalytic activity of bulk metals in electrochemical CO_2-reduction has been studied for decades based on the findings of Hori [11]. According to this work monometallic catalysts can be categorized based on the major type of product of CO_2-electroreduction. Group 1 consists of transition metals such as Fe, Ni, Pd and Pt, these metals tend to undergo HER. Au, Ag and Zn forms group 2, they predominantly catalyse CO-production during CO_2RR. Copper (and

some of its oxides) as group 3 has an exclusive catalytic nature due to the formation of various value-added hydrocarbons involving more than 2 electron transfer reactions. Lastly, group 4, the p-block metals (and their oxides), such as Sn, In, Bi and Pb, that primarily produce formic acid [3], [11]. Due to their relatively low cost and environmental compatibility, Sn and Bi are considered promising candidates for large-scale CO_2 reduction systems . [13].

Bulk Sn is known to selectively reduce carbon dioxide to formic acid, however studies[16], [40], [41] have proven that the catalytic performance of the metal is due to the surface oxide layer. The large overpotential to stabilize the key intermediate to form formic acid on the bare Sn surface appears to be lowered when SnO and SnO_2 is present on the surface. Although the standard reduction potentials for these oxides are considerably lower than the potentials required for carbon dioxide reduction reports are found about the existence of metastable metal oxide persistence during cathodic reactions [16]. Other than the oxide layer dependence it important to note that the performance of pure Sn as a catalyst is heavily dependent on the morphology [18], [19] as well. Nanoparticles have proven to deliver improved performance in the field of catalysis due to their increased surface area, which results in more exposed active catalytic sites. Some other study also suggests a higher density of grain boundaries in the polycrystalline electrode to also improve the performance [17], [35].

Bulk In-electrocatalysts for formate production are also widely employed, however studies have shown that the native oxide layer tends to impede the catalytic activity of this metal. It is also noteworthy that this metal out of the three utilized in this work is known to be the less effective for the cause. On the other hand efforts has been made to tune the performance of this metal, it was found that the removal of the native oxide layer still results in low FE values, but the anodization of the electrode to re-introduce indium oxide to the surface delivers improvements[3] ,[21].

Bi as electrocatalyst again is an attractive choice from an environmental and cost point of view as Sn. This metal is also abundantly available and has a low toxicity. The first report of Bi-based catalyst for carbon dioxide reduction was presented in the 90s, it was discovered to selectively catalyse formate production in aqueous $KHCO_3$ but did not receive much attention at that time, hence the next effort in studying the catalytic behavior of the metal was made in 2013 and focused on CO-production in ionic liquids. Since the concept of Bi-based catalyst for formate production is still in its early stages, it is deemed controversial whether the oxide layer for this metal creates a dependence on the performance of the catalyst. Studies have been rather focusing on the morphology control of the Bi-based catalysts to improve FE values [3] ,[21].

4.3.2. Bimetallic catalysts

As discussed briefly in the introduction the product selectivity of the metal-based catalysts is stemming from the nature of the key intermediate and their binding energies on the catalyst-surface and the competing HER due to the higher overpotentials CO_2-electroreduction requires. Incorporating a secondary metal to change the composition of the catalysts offers a way to tune the selectivity and activity through optimizing the binding strength of the intermediates on the catalytic surface and lower the overpotentials for the formation of formate.

Bimetallic catalysts can manifest in the form of alloy, intermetallic or nanocomposited structures. Within the group of alloy catalysts a further break down can be done to bulk alloys, surface alloys, near surface alloys and single atom alloys. Within nanocomposited structures there are groups such as nanodendrites and core-shell structured bimetallic nanoparticles [9]. The latter group is predominantly employed in homogeneous, while alloys are more likely being utilized in heterogenous catalysis. Bimetallic alloys can be synthesized in various ways such as electrodeposition, which was utilized in this work, co-precipitation, chemical vapor deposition (CVD), sol-gel process, mechanical alloying and atomic layer deposition (ALD) [14].
Through the specific intermetallic interaction on the catalyst surface the adsorption of the desired intermediate can be achieved more selectively which in result lowers the overall activation energy for formate production. The intermetallic interaction can be achieved by geometric effect, where the guest metal influences the surface coordination of the host metal atom on the surface providing new catalytic sites, which then results in enhanced surface area. This in general leads to increased active site exposure for interaction with the reactants. On the other hand this can also stabilize and strengthen the binding of those intermediates that can lead to other products than formate, and in result retains them from desorption, which enhances the selectivity of the catalyst[15].
Another type of interaction can be explained by the different electronic structure of the host and guest metal and orbital overlapping of the metal components. Through harmonic overlapping of the host metal orbitals with the guest metal orbitals a better interaction between the intermediate and the catalyst surface can be achieved. This overlapping has been more carefully studied with interaction of the p-orbital of a p-block metal with the d-orbital of a transition metal. In the case of both host and guest metal being p-block metals it was found that the d-orbital for instance of Sn-host still plays a role in stabilizing the key intermediate, according to computational results, the electron density from the more electronegative O-atom of a OCHO-intermediate is readily transferred to the d- and p-orbital of the Sn atoms, when the guest metal in a Sn-based catalyst is more electronegative than the host [13].

4. Experimental

4.1. List of Chemicals and Equipments

Table 2 List of Chemicals used during the thesis research

Chemical	CAS-Number	Supplier	Purity
Acetone	67-64-1	-	technical
Argon	7440-37-1	-	-
Bismuth Nitrate pentahydrate	10035-06-0	Thermo Scientific	98%
Carbon dioxide	124-38-9	-	-
Ethanol	64-17-5	-	technical
Ethanol	64-17-5	Chem-Lab	absolute
Isopropanol	67-63-0	-	technical
Indium chloride anhydrous	10025-82-8	abcr GmbH	98%
Indium nitrate hydrate	207398-97-8	Sigma Aldrich	99.5%
Nafion™	31175-20-9	Sigma Aldrich	5wt. % in lower aliphatic alcohols and water
Potassium chloride	7447-40-7	Baker	99.7 %
Potassium hydrogen carbonate	298-14-6	Acros Organics	>99.5 %
Sodium citrate dihydrate	6132-04-3	Baker	99.7 %
Tin	7440-31-5	Polymet	99.9 %
Tin chloride anhydrous	7772-99-8	Fisher Chemical	General purpose grade
Water	7732-18-5	-	-

Table 3 List of instruments and laboratory equipments used during the thesis research

Instrument	Modell	Supplier	Settings
Balance	-	Soehnle	-
Centrifuge	-	Sigma	
FT-IR	Spectrum 2	Perkin Elmer	ATR 4000-400 cm^{-1}
GC-TCD	Nexis GC-2030	Shimadzu	-
GC-BID	Nexis GC-2030	Shimadzu	-
Stirring plate	-	-	-
Microwave oven	Monowave 300	Anton Parr	-
Muffle oven	-	-	-
Potentiostat/Galvanostat	PGSTAT302N	Autolab	-
Potentiostat/Galvanostat	Palmsens4	Palmsens	-
Potentiostat/Galvanostat	2450 Source Meter	Keithley	Constant Current
Sonication bath	-	-	-
Sonication bath	-	-	-
Spectrophotometer	JASCO V-670	JASCO	DRS
XRD	XPERTII:PANalytical XPert Pro MPD	PANalytical	-
SEM/EDX	FEI Quanta 250 FEG/ Octane Elite 55	Quanta	5-20kV, 8.5mm WD

4.2. Electrode Preparation

The following sections contain the description of Sn-substrate cleaning and electrodeposition methods implemented as reported in literature with little modifications. All electrodes were created using 99,9% pure 0.5mm thick Sn plate cut into 2x1 and 3x1 cm pieces.

4.2.1. Blank Sn plates

Blank Sn electrodes were cut from Sn 99.9 purity Sn plate (0.5x100x150 mm) into 2x1 cm pieces. The plates were placed first into 2 V/V% Hellmanex solution and sonicated for 15 minutes, then the plates were rinsed off and the solution was exchanged to DI water and sonicated for an additional 15 minutes. Lastly, the DI water was replaced by technical

isopropanol and sonicated for one last time for 15 minutes. The plates were then transferred to a vial and stored under isopropanol until further use.

4.2.2. Sn-deposited Sn-plates

For the deposition solution 3.68 g of Na-citrate was dissolved completely in 250 ml DI water, and then followed the dissolution of 0.85 g Sn-chloride. This amount of precursor resulted in a 18mM solution. Prior the electrodeposition the solution was purged with nitrogen to reduce the chance of any side reactions while applying reducing currents. The galvanization process was carried out in a beaker with a clean Sn-plate as a working electrode and clean steel mesh as counter. Both electrodes were contacted to the Kethley 2400 sourcemeter via Cu-wire, carefully adjusting the electrodes to be parallel and to be submerged to the deposition solution to the same extent. Once the set-up was ready -4 mA fixed current was applied for different time windows. The deposition solution in the beaker was exchanged after each deposition to ensure constant source of precursors.

4.2.3. In-deposited Sn-plates

In- deposition solution was prepared dissolving 3.72 g KCl in 100ml DI water then adding 0.55 g $InCl_3$. The procedure involves the same deposition set-up as for Sn-deposition however, the applied current was set way higher, -18mA, in order to get In on the Sn-plates within foreseeable time. This way the reaction process took place in short amount of time. The deposition solution was exchanged after each reaction.

4.2.4. BiOI-deposited Sn-plates

Attempts were made to establish an electrodeposition method in water and organic solvent such as ethylene glycol for metallic bismuth, but due to the insolubility of most bismuth-compounds in water the depositions were unsuccessful for creating uniform films on the substrate. Acidic conditions to dissolve Bi-precursors in water also caused to re-dissolve the electrodeposited metal-spots from the Sn-plates. Ethylene glycol on the other hand was deemed to be more sufficient, however the highly viscous solvent resulted in Bi-islands on the Sn-plate, and electrocatalytic tests with these electrodes yielded insufficient amount formic acid in comparison to blank experiments.
To mitigate this issue analog to oxide derived Cu, BiOI was chosen to be electrodeposited on the substrate. This electrodeposition method is a well-known process in the research group therefore the implementation of it for this thesis project was logical and straightforward. In the concept of oxide derived copper, the oxidized metal is being reduced in-situ during the electrocatalysis. This reduction step has proven to significantly enhance the efficiency of the catalyst due to the presence of mixed oxidation states of copper.

Circling back, BiOI-deposited Sn-electrodes follows the preparation of $BiVO_4$ electrodes reported in T. W. Kim and K.-S. Choi's publication[5] until successful electrodeposition of BiOI using clean Sn-plates as substrate (WE), this procedure involves preparing a 0.04 M $Bi(NO_3)_3$ 5 H_2O and 0.4M KI aqueous solution acidified with concentrated nitric acid to pH 1.7. In a separate beaker p-benzoquinone was dissolved in absolute ethanol. Once all the solids in both containers have dissolved, the two mixtures were combined to obtain a dark reddish-brown

solution leaving brown tinting on the wall of the breaker, when the liquid is disturbed. In contrast to the publication, the electrodeposition set-up consists of Sn-plate as the cathode and a steel mesh as counter electrode, the utilization of a reference electrode is neglected. The potential was set to -1.5 V at each time, the deposition time was varied. Once the electrodes fully dried at room temperature they were then annealed at 130°C for 20h.

Before each experiment or electrochemical characterization process the electrode was placed in a small amount (ca. 10ml) of 0.5M $KHCO_3$ (electrolyte) overnight, which caused the BiOI layer to turn into $(BiO)_2CO_3$. This layer then during the electrochemical experiments was partially reduced to metallic Bi creating the alloy catalyst in situ.

4.3. Oxide Powder synthesis

After a statistical evaluation of CO_2-reduction experiments it was evident that the electrodeposition methods are not yielding high for formic acid amounts, and the new approach is to see whether oxide derived indium can enhance the performance of the In-Sn bimetallic electrodes. It has been proven that oxide derived Cu show improved performance for CO_2-reduction in comparison to metallic Cu, taking these findings into consideration In_2O_3-Sn electrodes were prepared to confirm the possibility of significant improvement with p-block metals as well[43].
As for Bi-Sn catalyst the process of employing BiOI as Bi-source did not yield sufficient amount of formic acid, regardless of it being oxide derived metal. The issue here could possibly stem from the preparation method, electrodeposition often leads to uniform films with minimal defects and lack of active sites. Different studies[44], [45] have been investigating the effect of heteroatom doping and defect concentration of bismuth subcarbonate, to promote enhanced photoactivity and higher efficiency for CO_2-reduction. Bi_2O_3-powder therefore was synthesized to promote improved formic acid production on the basis of these findings in the hope of achieving more complicated surface morphology and possibly higher defect concentration. Diversion from bismuth subcarbonate to bismuth oxide served to have stronger ground for comparison between In-Sn and Bi-Sn bimetallic catalysts.

4.3.1. Indium Oxide

The synthesis of Indium Oxide aims to follow research paper[42] where the authors have successfully produced nanoparticles of the material. While the experimental details in the paper are not too elaborate on the procedure, in some way it was manageable to establish a synthesis of the oxide nanoparticles. The starting point was to figure out their ratio of precursors in the reaction solution, with short calculations it came to be 1:1.42. The second step was to estimate the amount of product, which was set to ca. 100mg, with all these details then the synthesis followed the experimental section of the publication. 216.7 mg of $In(NO_3)_3$ hydrate was dissolved first in 12 ml ethanol forming a cloudy mixture then 145.1 mg of hexamethylenetetramine was added to the solution, stirred vigorously until the solution became homogenous.
The solution then was transferred to 30 ml microwave vial and placed into the Anton Paar instrument for 10 mins at 95 °C constant temperature. Once the hold time was over, active cooling to 55 °C followed.

The chalk white powder was transferred to centrifuge vials and the product was separated from the solvent, then washed with water, ethanol and acetone three times respectively. Lastly, the purified powder was dried at 100 °C in the oven over night.

4.3.2. Bismuth Oxide

40 ml aqueous solution containing 2mmol $Bi(NO_3)_3$ .5 H_2O and 3mmol Na_2SO_4 was prepared and stirred vigorously for 1h, while in a separate beaker another 40ml of solution was prepared of 18mmol of NaOH. Once the 1h has passed the NaOH solution was added dropwise to the $Bi(NO_3)_3$- Na_2SO_4 mixture. After an additional 10mins of stirring the now 80ml reaction solution was transferred in smaller portion (10-12ml each time) into a 30ml microwave vial and left to form the oxide powder in the reactor at 100 °C for 15 mins. The product was separated from the solution using centrifuge and washed with DI water and ethanol three times respectively. The pale-green-yellow powder was dried overnight at 80 °C in the drying oven.

4.3.3. Electrode preparation

Using the oxide powders two inks were prepared for electrode fabrications with drop-casting method. 10mg/ml of oxide powder with 1µL Nafion/ mg catalyst were dispersed in Isopropanol and applied onto 2x1cm Sn-plates in three layers, 20 µL of ink at each time. The layers were left to dry inbetween. The electrodes were ready to be implemented after complete evaporation of the solvent. Formation of bimetallic catalysts using oxides on the Sn-plates were then the result of the reducing potentials applied during the electrochemical CO_2-recution. Therefore, the bimetallic electrodes were created in-situ during the chronoamperometric experiment.

4.4. Characterization Methods of the Electrodes

The following section briefly describes the characterization methods used on the fabricated electrodes and the synthesized oxide powders. in terms of structure, and electrochemical nature

4.4.1. Electrochemical Methods

Electrochemical characterization measurements were completed under nitrogen and carbon dioxide atmosphere before each chronoamperometric experiment to confirm the catalytic activity of the electrodes. The electrolysis setup involved an H-cell equipped with septa for both liquid and gaseous samples to obtain on the working electrode side. The working electrodes were the materials of interest, with Ag/AgCl reference electrode connected in the same chamber. On the counter side for all measurements, Pt-electrode was utilized. For all experiments, both sides of the chambers were filled with 45 ml 0.5M $KHCO_3$ solution as electrolyte, and the working electrode side was purged for 1 hour first with nitrogen to ensure oxygen-free environment. Presence of oxygen can lead to unwanted side reactions at the potential range of the measurements causing disturbance in the Faradaic efficiency values, and possibly damage in the catalyst, which again falsifies the conversion rates. Nitrogen-

purging was followed by an additional hour of CO_2- saturation of the cell, for the formate production.

Once the purging was done, the cell was connected to the potentiostat, and LSV (Linear Sweep Voltammetry) and CV (Cyclic Voltammetry) scans and eventually chronoamperometry were performed. During this thesis project two different devices were employed for the measurements, they are listed in section 4.1, for the ease of discussion these two instruments will be referred to as Autolab and Palmsens.

The conversion of the potential values from Ag/AgCl- reference electrodes to RHE adjusted to the pH of the electrolyte is directly calculated from the Nernst-equation expressed as a function of pH:

$$E = E^0 + \frac{R \cdot T}{z \cdot F} \cdot ln \frac{a_{ox}}{a_{red}}$$

R… ideal gas constant [R=8.314 Jmol/K^{-1}]
T…temperature [298 K at standard conditions]
F…Faraday constant [96485 C mol^{-1}]
z…number of transferred electrons

Where:

$$\frac{R \cdot T}{z \cdot F} = 0.059V$$

Using the pH value of the electrolyte, the conversion of the potentials follows the equation below:

$$E_{RHE} = E^0_{Ag/AgCl} + (pH \cdot 0.059) + E_{Ag/AgCl}$$

E_{RHE}… potential vs. RHE [V]
$E^0_{Ag/AgCl}$… standard potential of the Ag/AgCl/3M KCl electrode at pH 7, standard ambient temperature and pressure (SATP) [$E^0_{Ag/AgCl}$ =0.21V]
$E_{Ag/AgCl}$… potential vs. Ag/AgCl/3M KCl electrode [V]

Linear Sweep Voltammetry

After successful assembly of the electrochemical cells for CO_2RR linear sweep voltammetric measurements followed each round of purging, first under nitrogen atmosphere, then an hour of CO_2-purging, and another LSV measurement. All LSV- curves were recorded from 0 to -1.1 V (vs. RHE), with 0.05 V/s scan rate.

Cyclic Voltammetry

Cyclic voltammetry was done after each LSV measurement additionally, the potential range was again between 0 and -1.1 V (vs. RHE) with a scan rate of 0.05 V/s. For each sample 3 cycle scans were acquired, under both nitrogen and carbon dioxide. This scan rate enables to detect redox processes of electroactive species that depend highly on diffusion in the electrolyte to the electrode surface. Moreover, this scan rate allows certain redox peaks to be more defined or even some instances distinguished in case some processes are taking place at potential values lying close to one another.

4.4.2. X-ray Diffraction

Sn plates and electrodes were placed in the sample holder using adhesives and levelled out to be in plane with the edge of the holders. Powder samples were placed on Si- wafer (orientation) and fixed with vaseline. The samples were then placed to be measured via autosampler in a PANanalytical X'pert Pro multi-purpose diffractometer. Cu-anode served as an X-ray source, with primary beam of 2:1 K_α and K_β (8.04 keV, 1.5406 Å).The measurement configuration was set to Bragg Brentano geometry- sample fixed in the center rotating along the z-axis while detector and source are moving along the goniometer circle at the same rate- the program was a short 21min scan, from 5 to 90 degrees.

4.4.3. Attenuated total reflection Fourier transformed infrared spectroscopy (ATR-FTIR)

In-oxide powder characterization was done by FT-IR measurements, prior to the scans a background spectrum of air was recorded, then few milligrams of the powders were place onto the diamond and pressed. The spectrum was recorded for each sample in the range of 4000-400 cm^{-1} in ATR setting.

4.4.4. Scanning electron microscopy and Energy dispersive X-ray Spectrometry

SEM/EDX measurements were done by Jakob Blaschke on FEI Quanta 250 FEG with acceleration voltage of 5kV for imaging and 20kV for EDX scans with 8.5mm working distance. EDX scans were performed with the same instrument which is equipped with a EDAX-AMETEK Octane Elite 55 detector.

4.5. Catalytic Performance testing

Catalytic performance testing of the electrodes was conducted via electrochemical CO_2RR at different applied potentials. The products forming in the headspace were analyzed by gas chromatography, while liquid products were detected and quantified using H-NMR.

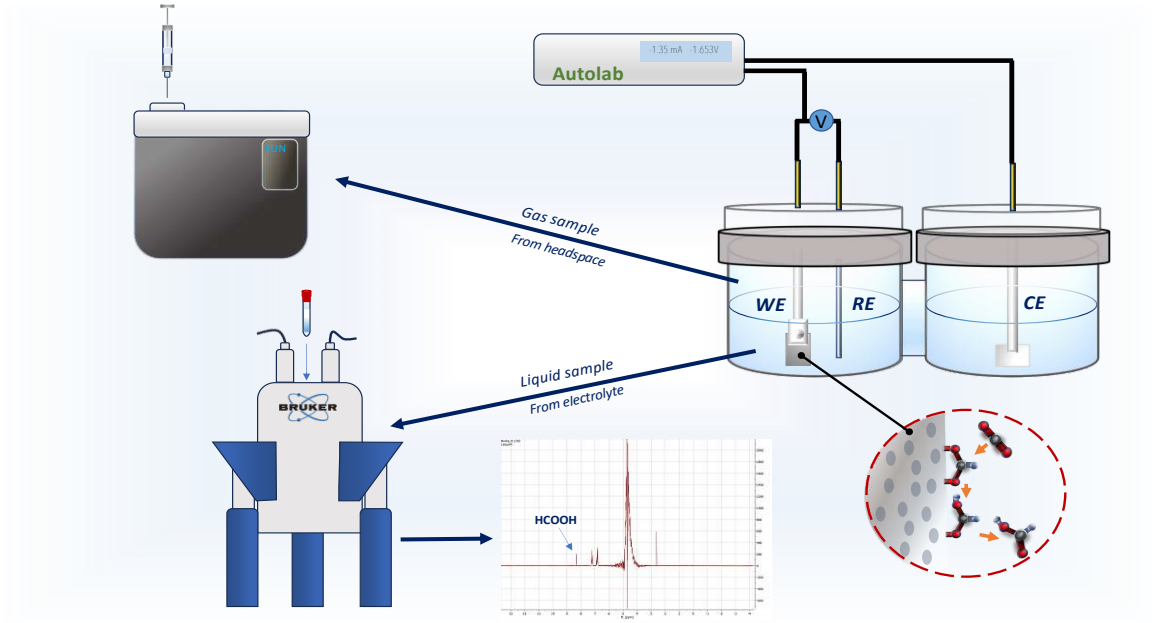

Figure 2 Scheme of the workflow for catalytic performance testing

4.5.1. Electrocatalytic CO_2RR

As previously mentioned, the electrolyte for all experiments was a 0.5M $KHCO_3$ solution, in both chambers of the H-cell, due to the lower solubility of carbon dioxide in aqueous medium this solution also acts as an additional source of CO_2 in the liquid phase. Working electrode side contained the electrode of interest, the catalyst, and an Ag/AgCl reference electrode as well as a magnetic stirring bar, while the counter electrode side was equipped with a Pt-electrode.
The cell sealed on both sides and purged first with nitrogen on the working electrode side for 1h, ensuring oxygen-free conditions, then saturated an additional hour with CO_2.
After saturation, the cell was connected to a potentiostat and constant potential was applied for 1h, while the electrolyte of the cathodic side was stirred. The potentials applied were -1V, -0.9V, and -0.8V vs. RHE.
For Faradaic efficiency evaluation, obtained *I vs. t* graph was integrated to define the amount of charge involved in the reduction of CO_2 or eventually in water splitting as a competing reaction at the chosen potentials.

4.5.2. Gas Chromatography

After the chronoamperometric measurements, gas sample was drawn from the headspace of the working electrode side using a luer-lock syringe and analysed using Shimadzu Nexis GC 2030 at a column temperature of 40 °C. In the laboratory 2 of these instruments are available, one is equipped with a TCD detector while the other with a BID detector.
In some cases, the amount of Hydrogen was below the detection limit of TCD. In this case, another Shimadzu Nexis 2030 which is equipped with a barrier ionization discharge (BID) detector was used.

4.5.3. NMR

The liquid products, mainly formic acid (in the form of formate), was detected and quantified in a 250Hz H-NMR using water suppression using deuterium lock. This in practice suppresses the high intensity peak coming from the high amount of water in the sample so the other analytes in the sample become quantifiable. The samples for this analysis consisted of 700 µL of the electrolyte from the cathodic side of the reactor, mixed into it an internal standard, containing 50 mM concertation of phenol and 10 mM DMSO in D_2O. These two chemicals tend to not interfere with any other products formed in the CO_2RR. Peaks showing up at higher ppm shifts were then integrated relatively to the phenol peaks, and the ones at lower shifts were quantified via the DMSO peak.

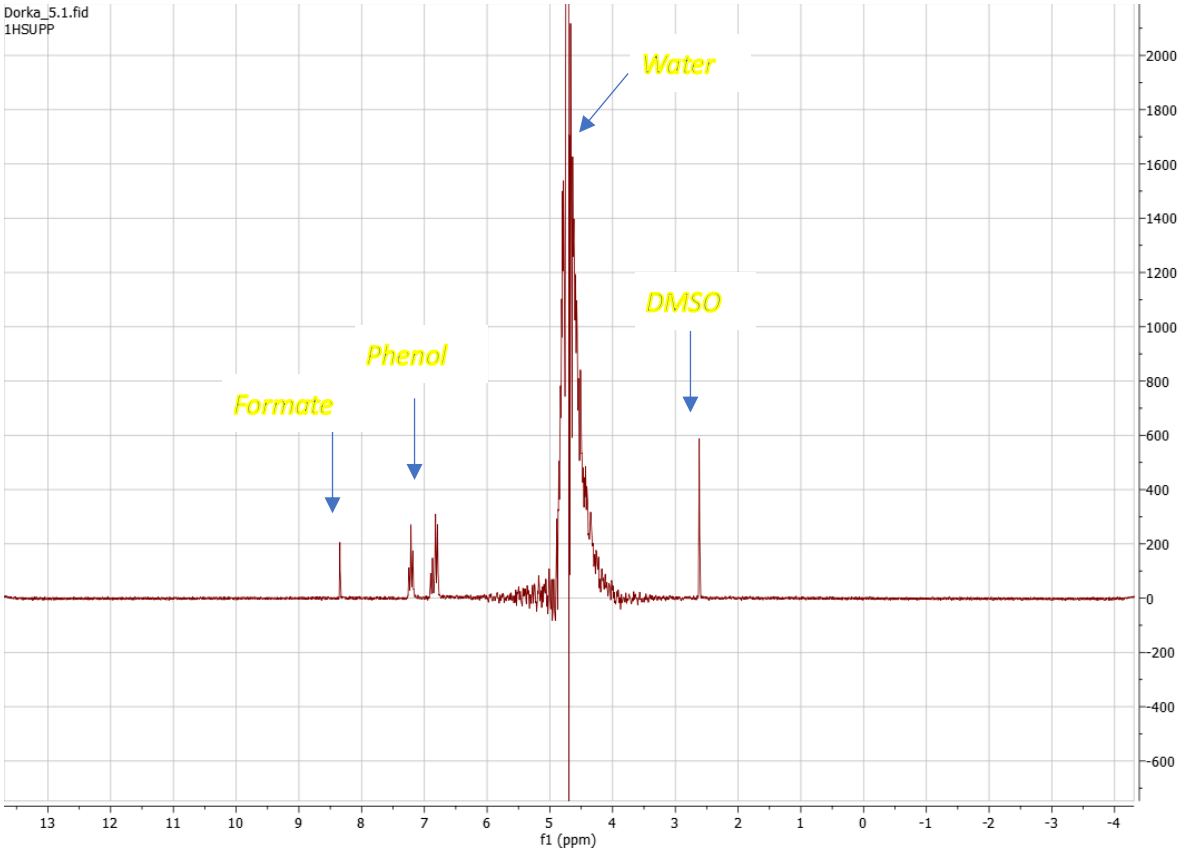

Figure 3 NMR-spectra of an electrolyte sample obtained after CO_2RR experiment using In-deposited Sn-plate as working electrode

4.5.4. Faraday Efficiency calculation

Faradaic efficiency is one of the key parameters to describe the performance of a catalyst in electrochemical CO_2 reduction, alongside current density, overpotential and durability. This parameter also directly points towards the selectivity of particular product forming during the electrocatalysis. Mathematically it is calculated using the following formula:

$$FE(\%)=\frac{Q_{product}}{Q_{total}} \cdot 100\%$$

FE(%)…Faraday efficiency [%]
$Q_{product}$...charge consumed for the generation of a particular product
Q_{total}…total charge transferred during the electrolysis

Where Q_{total} is determined using the integrate of the chronoamperometric plot on the basis of:

$$Q = I \cdot t$$

Q…electric charge [C]
I…electric current [A]
t…time [s]

Calculation of $Q_{product}$ follows:

$$Q_{product} = n_{product} \cdot z \cdot F$$

$Q_{product}$… charge consumed for the generation of a particular product
$n_{product}$…Amount of product expressed in mols t…time [s]
z…number of transferred electrons [2 in the case of HCOOH]

The amount of products depends on the state of matter, the concentration of gaseous products in the headspace is determined using gas chromatography. The GC results are expressed in ppm, the conversion of the values into moles is done via:

$$n=\frac{ppmproduct \cdot V_{headspace}}{10^6 \cdot V_{idealgas}} \cdot 100\%$$

ppm…parts per million of product [H_2, CO, HCOOH]
$V_{headspace}$…Headspace volume of the working electrode side of the H-cell
$V_{ideal\ gas}$… ideal gas volume at 296K [$V_{ideal\ gas}$=24.62 L]

For liquid products the calculation is facilitated through the integration of the NMR peaks. As previously described formate peak appears at higher ppm shifts, therefore the relative integral to this peak will be determined through the phenol peaks. Once the values are obtained the formula follows as:

$$C_x = \frac{I_X}{I_{cal}} \cdot \frac{N_{cal}}{N_x} \cdot C_{cal}$$

I_x…Integral area of the product peak
I_{cal}…Integral area of the internal standard peak
N_x…Number of nuclei giving rise to the signal in the compound of interest [1 for HCOOH]
N_{cal}…Number of nuclei giving rise to the signal in the internal standard [5 for Phenol, 6 for DMSO]

C_{cal}…Concentration of the internal standard in the sample

which will lead to the concentration of the product C_x within the NMR tube. The concentration in the original electrolyte is then calculated by a simple equation of dilution:

$$C_{45ml} = \frac{C_x \cdot 0.74}{0.7}$$

C_{45ml}…Concentration of the product in 45ml

0.74 for the sample volume in the NMR-tube including the internal standard, which in this case dilutes the sample and 0.7 for the volume of the electrolyte without the standard.

From this concentration the total amount of product is calculated:

$$n_{product} = c_{45ml} \cdot 45ml \cdot 10^{-6}$$

$n_{product}$…Amount of product expressed in mols

And the mols of electrons:

$$n_{electrons} = n_{product} \cdot z$$

$n_{electrons}$…mols of electrons consumed generating the product of interest
z…number of transferred electrons [2 in the case of HCOOH]

The total amount of electrons transferred through the electrolysis:

$$n_{totalelectrons} = \frac{Q_{total}}{F}$$

Q_{total}…total charge transferred during the electrolysis
F…Faraday constant [96485 C mol^{-1}]

The charge in the Faraday efficiency formula is then replaced by the number of electrons:

$$FE(\%) = \frac{Q_{product}}{Q_{total}} \cdot 100\% = \frac{n \cdot z}{Q/F} \cdot 100\% = \frac{n_{electrons}}{n_{totalelectrons}} \cdot 100\%$$

FE(%)…Faraday efficiency [%]
$Q_{product}$…charge consumed for the generation of a particular product
Q_{total}…total charge transferred during the electrolysis
z…number of transferred electrons
F…Faraday constant [96485 C mol^{-1}]
$n_{electrons}$…mols of electrons consumed generating the product of interest
$n_{total\ electrons}$….total amount of electrons transferred during the electrolysis

5. Results and Discussion

5.1 Characterization of the electrodes

This section presents the results and their interpretation regarding the fabricated electrodes. These methods provide insights into the electrochemical behavior, as well as the structure and composition of the material.

5.1.1. Electrochemical Methods

As mentioned in the previous chapter to investigate the electrodes, linear and cyclic voltammetry was utilized with the measurement parameters listed in the respective section.

Linear Sweep Voltammetry

Linear sweep voltammetry involves applying a linearly increasing or decreasing potential to an electrochemical cell while measuring the resulting current response, providing insights into the redox processes occurring at the electrode surface.

The next sections present the voltammograms of each sample type under CO_2 and N_2 atmosphere, at the same applied potential range of -1.1V to 0V vs. RHE.

Blank Sn plate

As suggested earlier, this method offers a deeper insight into the redox processes occurring on the electrode surface.

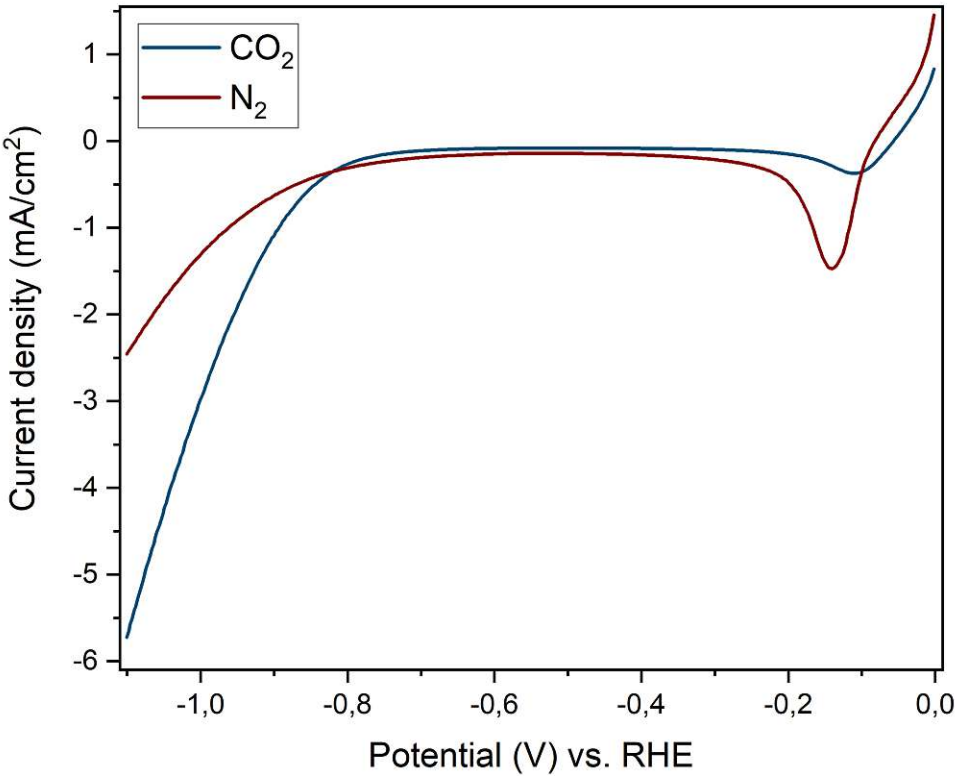

Figure 4 Linear sweep voltammetry curves of a blank Sn-plate after N_2 (red) and CO_2 (blue) purging.

The initial Linear Sweep Voltammetry (LSV) measurements were conducted for each sample following purging with nitrogen. Upon examination of the voltammogram, it becomes evident that the electrode surface underwent reduction at approximately -0.1V, as indicated by the peak. Matching with the standard electrode potential values this could be a reduction of SnO_2 to alpha-SnO.

Moving on to the second curve, under CO_2 saturation, the same peak shifted to even lower potentials and appears less defined. This implies that the electrode surface now contains fewer reducible species or that the presence of carbon dioxide offers greater resistance to their reduction.

A more significant increase in current for both curves begins to occur only after reaching ca. -0.8V. The higher reduction current observed under carbon dioxide also confirms the Sn-plate's electrocatalytic activity.

Sn deposited Sn plates

The electrodeposition of Sn onto Sn-plates aimed to discern whether the presence of a pure Sn-phase enhances catalytic performance compared to a simple Sn-plate with a native oxide layer.

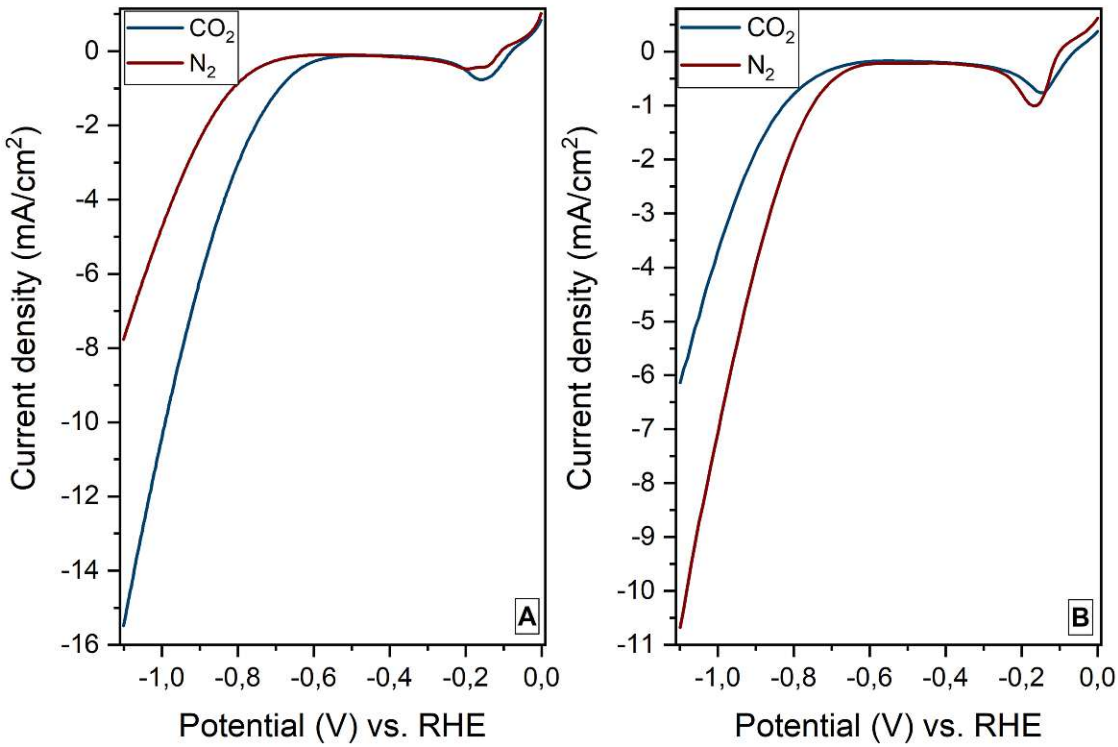

Figure 5 Linear Sweep voltammetry curves of Sn-deposited Sn-plates, 1min deposition time (A), 1.5min deposition time (B)

However, it is apparent that identical peaks persist at similar potentials (approximately -0.1V), as observed with a standard Sn-plate electrode.
Electrodeposition with a reaction time of 1min appears to diminish the presence of these species on the surface, resulting in a 2.5-fold increase in reduction currents. Conversely, a deposition time of 1.5min leads to an adverse effect on reduction current, with increased values observed under a nitrogen atmosphere, while maintaining similar performance to a blank Sn-plate under carbon dioxide.

In deposited Sn plates

In the case of indium-deposited Sn-plates, three different types of samples were prepared due to variations in the electrodeposition solution. Initially, the solution resulted in a clear homogeneous mixture only on the first attempt. Subsequent attempts yielded an opaque solution, despite multiple retries. Nevertheless, this opaque solution was still used for electrode fabrication, as the resulting layer did not visibly differ from the original ones.

After further testing of the deposition solution it was found that residues of carbonate or alkaline salts can cause the indium ions in the solution to precipitate, as both indium-hydroxide

and indium-carbonate are insoluble in water at pH 6 and above. The opacity of the solution was not to a disturbing extent; therefore, the pH of the solution was not modified, also to avoid oxidizing the surface of the Sn-plate. Residues of these species can easily occur in the laboratory the measurements were conducted, as the group deals with potassium-carbonate electrolyte, also used during this thesis project, potassium-hydroxide also as electrolyte. Very small amount from glassware, spatula, tubing used for purging the solution can disturb the equilibrium of ions in the deposition solution, causing precipitation.

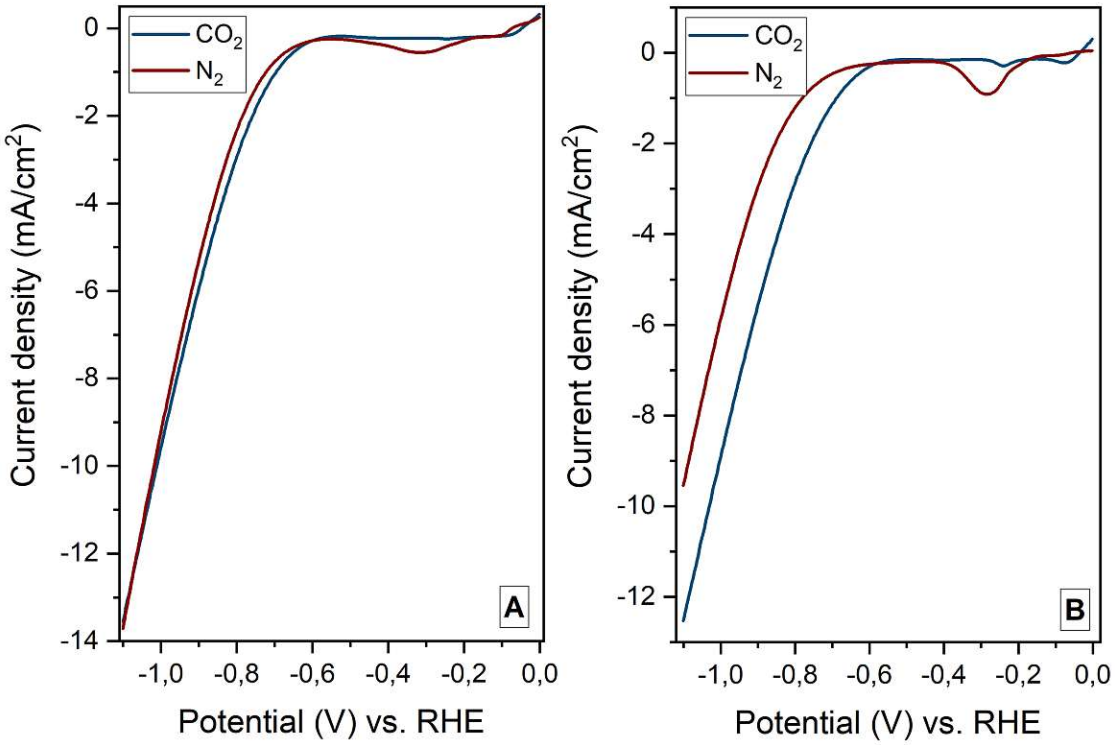

Figure 6 LSV curves of In-deposited Sn plates, both with the deposition time of 45s, A, resulting from a clear deposition solution, while B from an opaque solution

This difference in the deposition solution seemingly led to a broadening of the peak at lower potentials compared to its opaque counterpart of the same sample type. Furthermore, the redox reaction peak shifted to higher potentials compared to the one observed with the blank Sn-plate, which corresponds well with the standard electrode potential of In^{3+} reduction to In(s). Under a carbon dioxide atmosphere, this peak almost completely faded away, indicating a higher energy barrier for the redox reaction to occur in a carbon dioxide-saturated electrolyte, or a substantial loss of reducible species on the electrode surface following an initial LSV measurement in a nitrogen atmosphere. Notably, the CO_2-curve exhibited a steeper slope in both cases, confirming increased catalytic activity in the presence of the reductant.

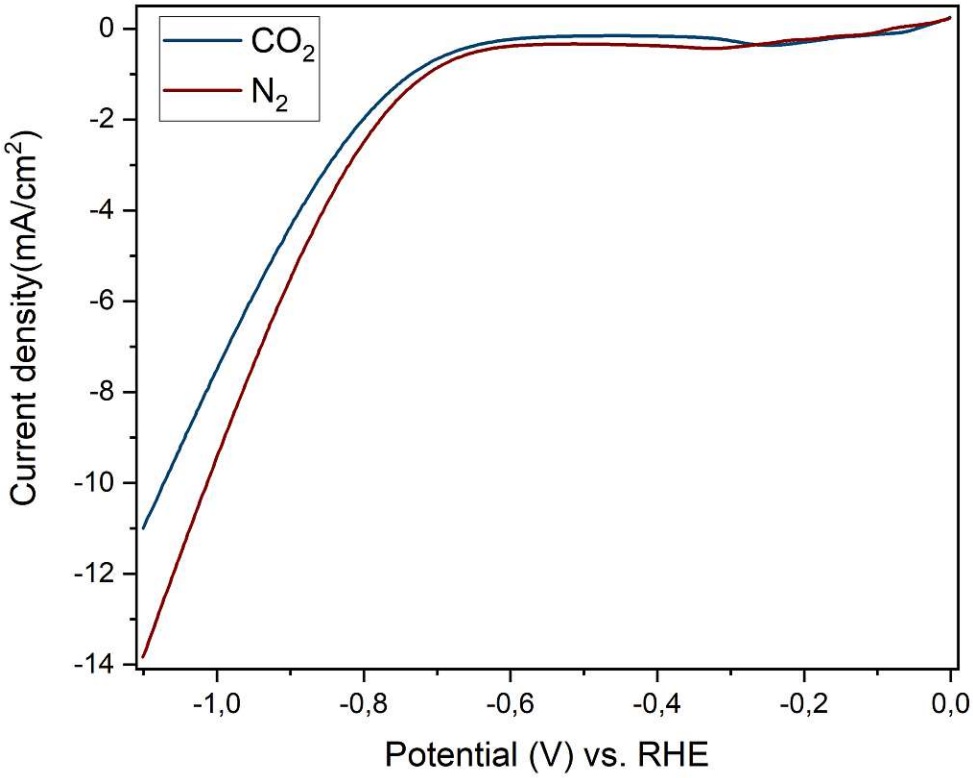

Figure 7 LSV curve of an In-deposited Sn-plate with 55s reaction time from an opaque solution

In the case of the sample with a 55-second deposition time, two main observations were made: firstly, the redox reaction peak at lower potentials appeared even flatter, and secondly, the presence of CO_2 did not enhance the current response as significantly as observed in the other two samples.

BiOI deposited Sn plates

With BiOI samples, it's evident that even a slight difference in deposition time resulted in distinct types of samples. However, it's important to acknowledge the numerous factors involved in the electrode preparation method, which could potentially lead to variations in each sample's behavior. Consequently, each sample exhibited unique LSV curves.

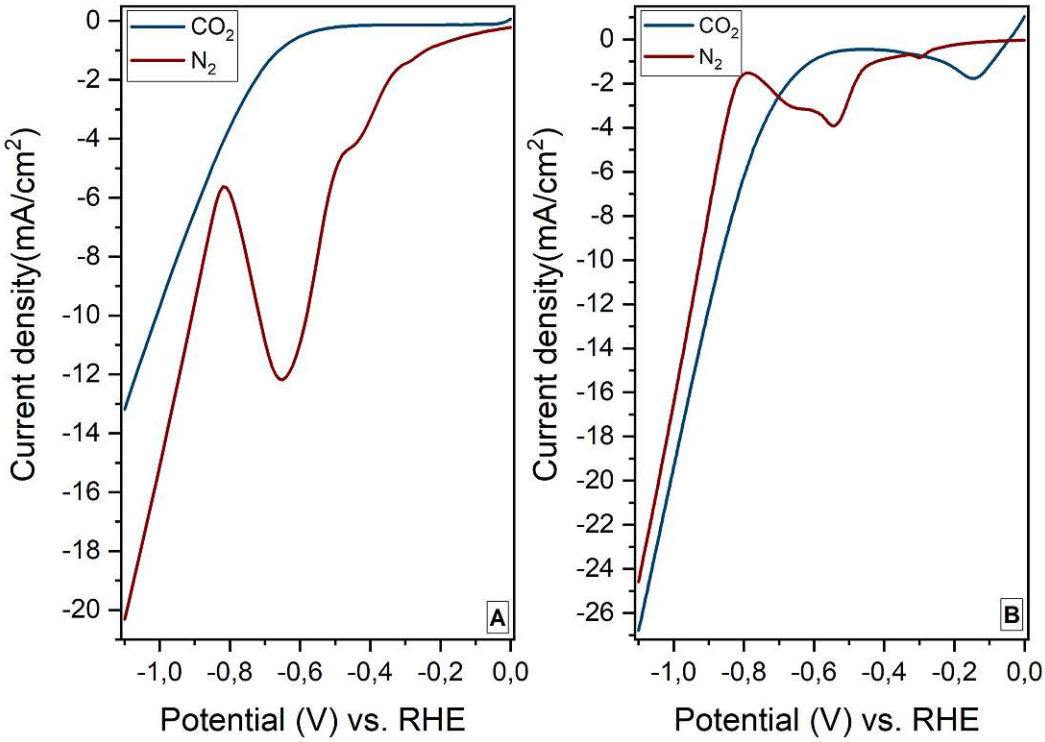

Figure 8 LSV measurement results of BiOI-deposited Sn-plates, A, 2min deposition time, B, 3min deposition time

A consistent observation across these curves is the onset of current increase under a CO_2 atmosphere at approximately -0.7V, along with the emergence of a well-defined redox peak at -0.5-0.6V under a nitrogen atmosphere, which can be related to Bi_2O_3 -reduction with 6 electron transfer. However, it's noteworthy that while the shape of this curve may not be uniform, the appearance of the peaks is at the same potentials, hence both samples undergoes the same reduction process. After CO_2-purging the sample with 3 min deposition time reveal another peak at approximately -0.1V which again highly likely comes from SnO_2 to alpha-SnO reduction of the substrate.

Metal-oxide drop-casted Sn plates

Utilizing metal oxides as a source for the secondary metal in bimetallic catalyst compositions entails the understanding that the introduced layer will undergo partial reduction.

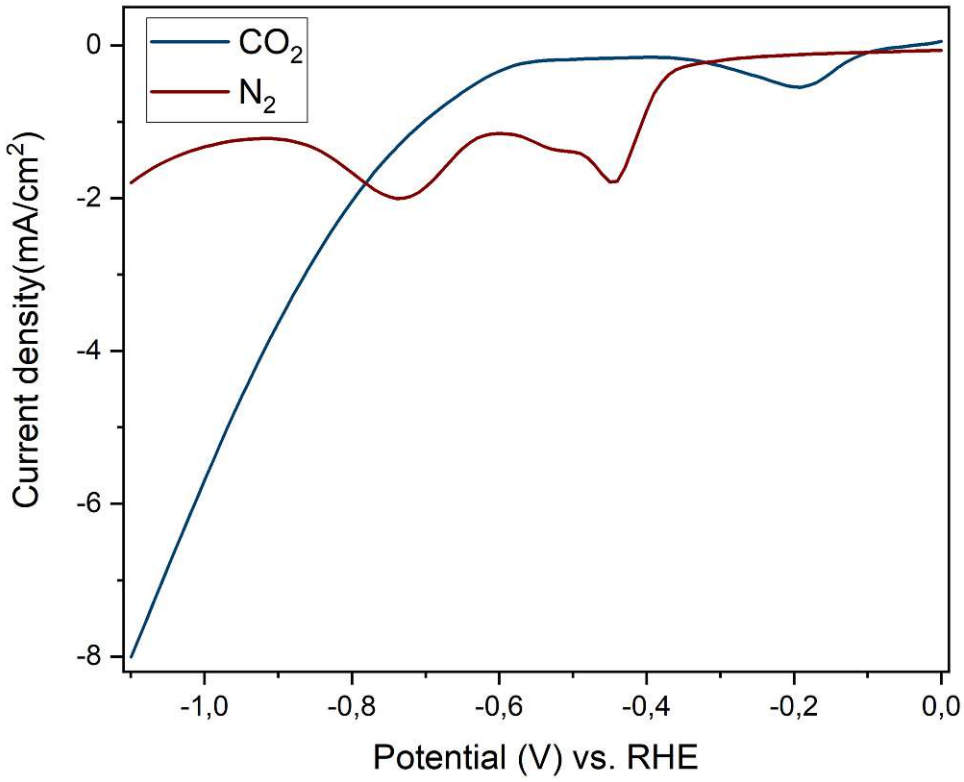

Figure 9 LSV curve of an In_2O_3 dropcasted Sn-plate

This is evident from the initial sweep, where it's apparent that a 2- electron transfer reaction from In^{3+} to In^{+} occurs, which cannot be further observed under a carbon dioxide atmosphere. Interestingly, the CO_2 curve for the In-oxide powder closely resembles the curve of a blank Sn-plate, adversely to the BiOI-samples here this peak can be also matched up with another electron transfer reaction for In^{+} to metallic In, aside from the tin oxide reducton process. Broadening of this peak means this reaction took place at a slower rate in comparison to the 2-electron transfers after N_2-purging.

The Bi-oxide layer undergoes major reduction processes during the initial Linear Sweep Voltammetry (LSV) measurement under nitrogen, similar to the In-oxide.

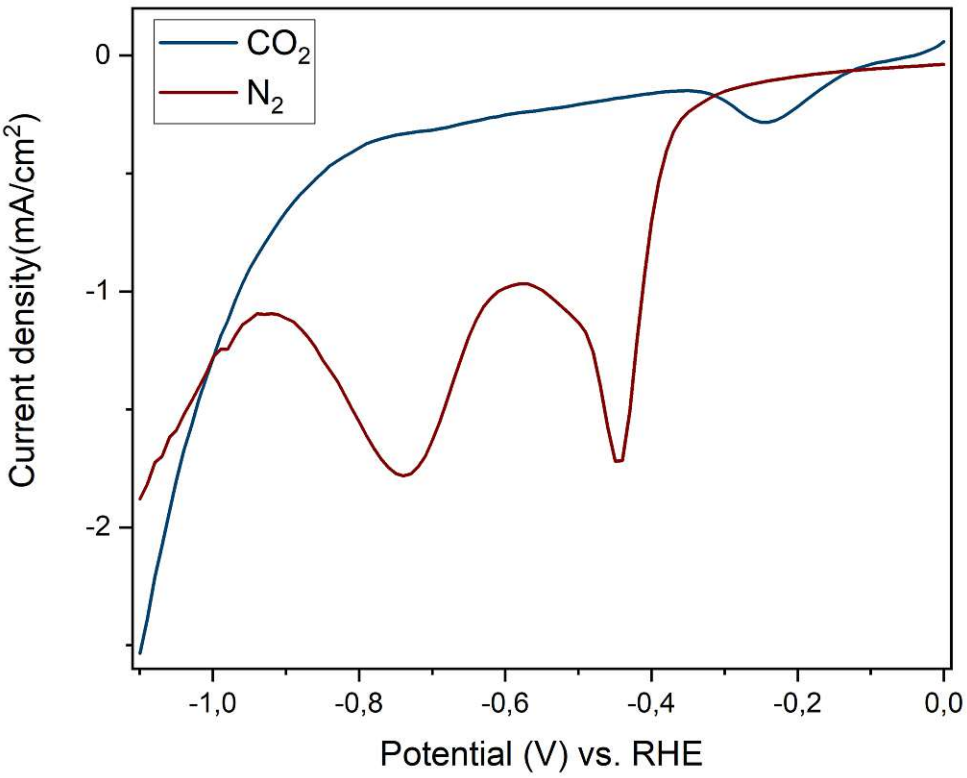

Figure 10 LSV curve a Bi2O3 dropcasted Sn-plate

However, in this instance, the peaks are more defined, possibly due to differences in particle sizes. The synthesized In-oxide powder comprises nanoparticles, whereas the Bi-oxide powder is a regular crystalline material identifiable through X-ray powder diffraction, as discussed in a subsequent section of this thesis. Sharp peak around -0.4V can be matched up with the 6-electron transfer reaction of bismuth oxide to metallic bismuth. The following peak around -0.75V assumably still belongs to the same reaction of bismuth oxide, but due to the lower scan rate of the measurement it enabled some intermediates to stabilize therefore the peak shifted. After purging with CO_2 the recurring peak of tin oxide can be observed again. Onset of the current increase in the case of Bi-oxide has shifted to lower potentials in comparison to In-oxide-Sn-electrode, which could not be observed with BiOI-deposited samples, therefore it can be assumed that this electrode contains not only purely metallic phases, but some residues of oxides as well.

Cyclic Voltammetry

Cyclic voltammetry entails cyclically varying the potential applied to an electrochemical cell while monitoring the resulting current, in opposition to linear sweep voltammetry this method provides detailed information about the reversible and irreversible redox reactions at the electrode interface.

The next sections present the voltammograms of each sample type under CO_2 and N_2 atmosphere displaying only the first and the third cycle, at the same applied potential range of -1.1V to 0V vs. RHE.

Blank Sn plate

Apart from Linear Sweep Voltammetry, additional valuable insights, such as reaction reversibility, can be obtained using cyclic voltammetry. When observing the curves obtained from a Sn-plate, it becomes apparent that the redox reaction of SnO_2 to alpha-SnO at lower potentials is reversible. The current signal to this peak also progressively gets lower with increasing cycles. The separation between the reduction and oxidation peaks suggests that electron transfer for oxidation occurs at a higher rate compared to reduction.
Furthermore, there is an increase in reduction current at the lowest scanning potential during the 3rd cycle compared to the 1st cycle.

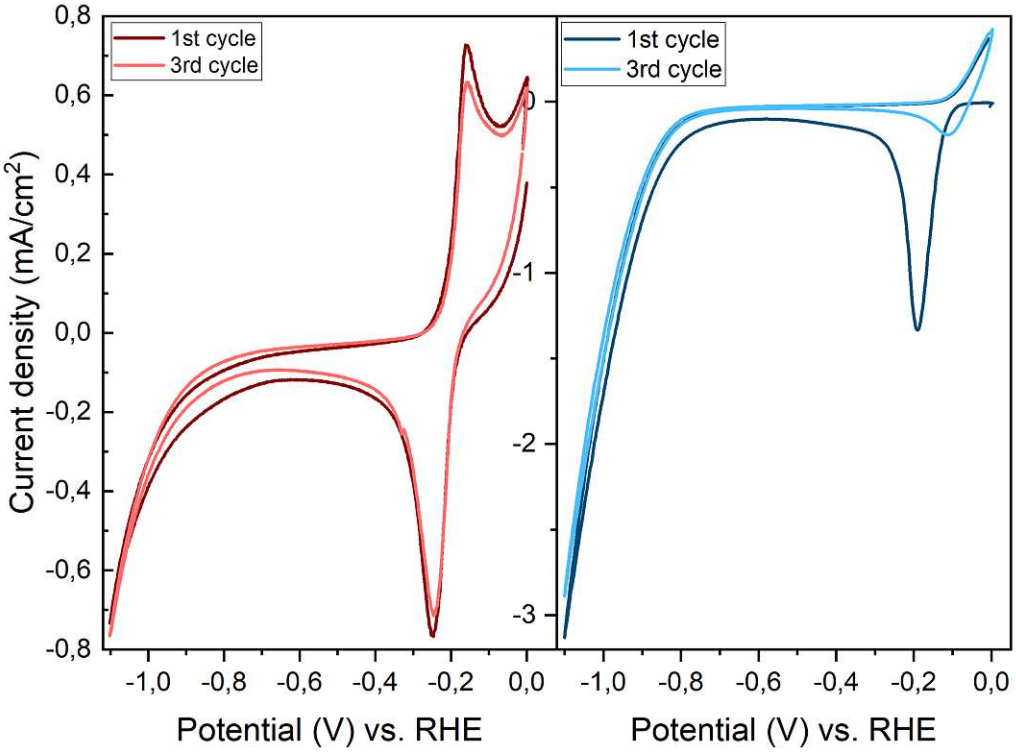

Figure 11 Cyclic voltammetry scans of a blank Sn-plate under nitrogen (red) and under carbon dioxide (blue)

Purging with carbon dioxide did not have the same effect on the reduction current at the lowest scanning potential through the 3 cycles. However, the hysteresis in the 3rd cycle suggests lowered activation barriers for electrochemical reactions on the surface in comparison to the 1st cycle.

Sn deposited Sn plates

Sn-deposited Sn plates exhibit the same reversible reaction at lower potentials as the blank Sn-plate. However, under a nitrogen atmosphere, the separation between peaks has increased. Additionally, the multielectron transfer peak of the first cycle appears less defined for both samples, eventually merging into a singular peak by the 3rd cycle. Notably, the reduction current follows a similar trend under nitrogen, indicating increased conductivity by the 3rd cycle for both samples. Despite the 1.5min deposition time yielding less current than a 1min deposition time sample, it still achieves higher values compared to the blank sample.

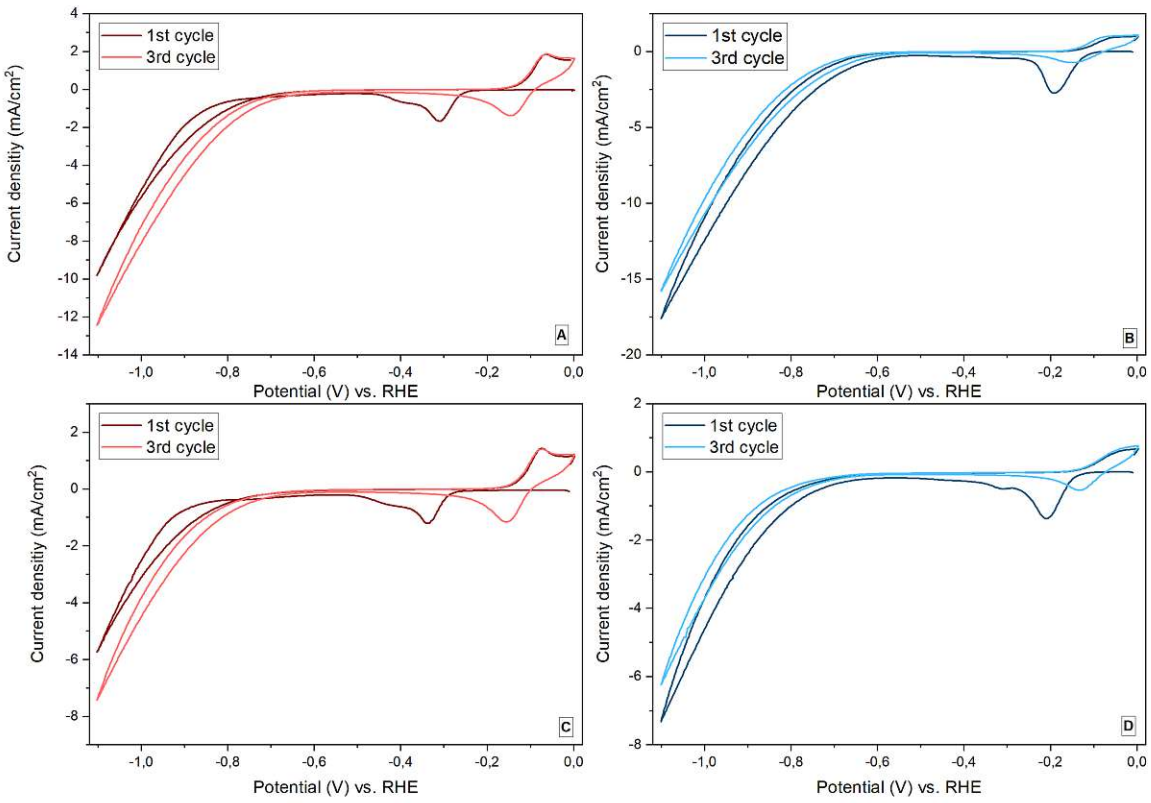

Figure 12 CV scans of Sn-deposited Sn plates with a deposition time of 1 min (A,B) and 1.5 min (C,D) under nitrogen (red) and carbon dioxide (blue)

Under carbon dioxide, the peak of the same reversible reaction became smaller in both the forward and reverse scans. Interestingly, the sample with a 1.5min deposition time appears to have maintained the peak shape during the 1st cycle, eventually merging into a single peak by the 3rd cycle. Moreover, the reduction current follows a similar trend to the blank sample, exhibiting decreased current values by the 3rd cycle and lowered activation barriers during the reverse scan.

In deposited Sn plates

As discussed in the Linear Sweep Voltammetry section, In-deposited Sn-electrodes exhibit three distinct sample types characterized by differences in deposition solutions (clear and opaque) and deposition times (45s and 55s).
In the LSV scans of these samples, it was evident that the peak at lower potentials appeared broader and less defined compared to the blank sample. Notably, the peak separation between the forward and reverse scans maintained the same extent as observed with Sn-deposited Sn-electrodes. Reduction current under nitrogen increased by the 3rd cycle, with current values higher compared to a blank sample.
However, in CV scans under carbon dioxide, there was a drop in current values by the 3rd cycle, consistent with previous CV curves. Additionally, the reversible reaction peak under a carbon dioxide atmosphere almost completely flattened out during the reverse scan.

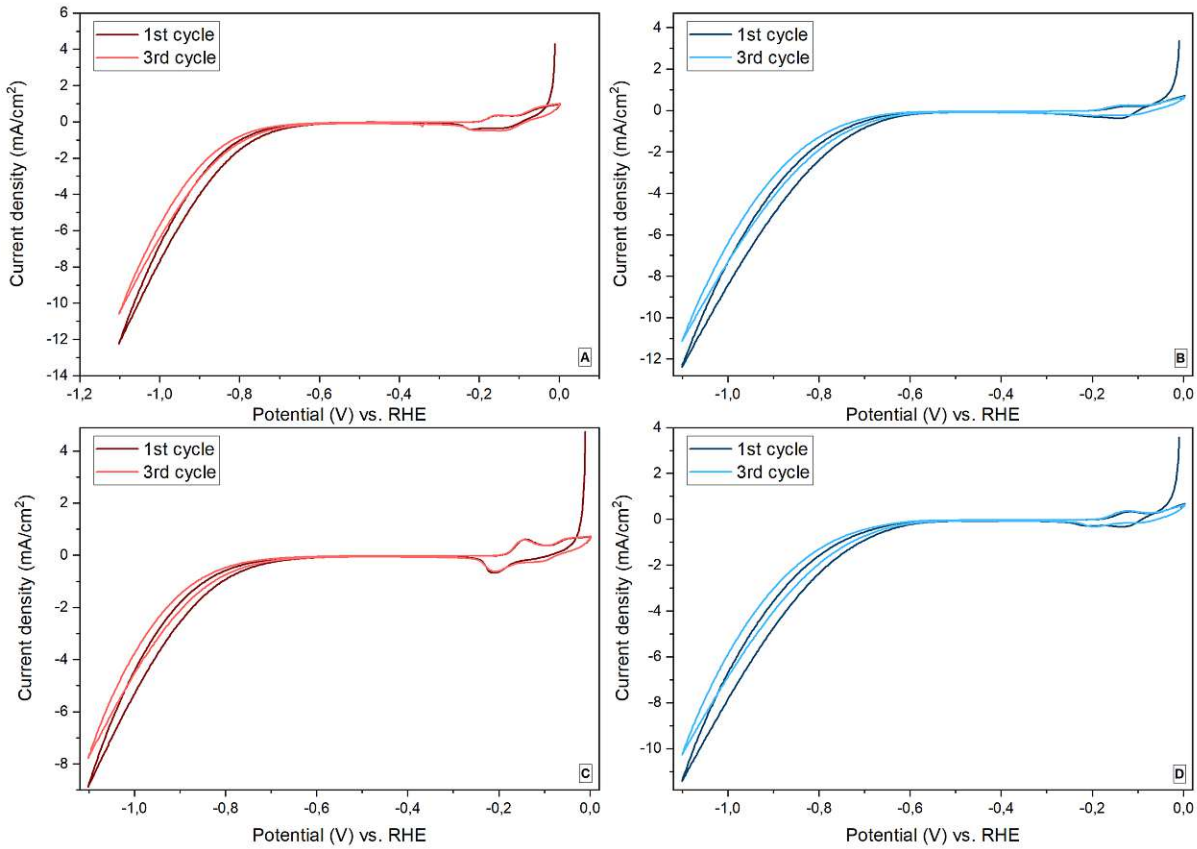

Figure 13 CV scans of In deposited Sn-plates with 45s deposition time from clear deposition solution (A,B) and from an opaque solution (C,D) under nitrogen (red) and carbon dioxide atmosphere (blue)

The sample derived from the opaque solution exhibits more defined peaks in both scans under nitrogen and carbon dioxide atmospheres. This could potentially be attributed to the presence of a different surface structure that is more prone to reduction at that potential. Different surface structure of the electrodes can be caused by changed kinetics of the electrodeposition process due to the presence of minimal amount of precipitation of In-species.

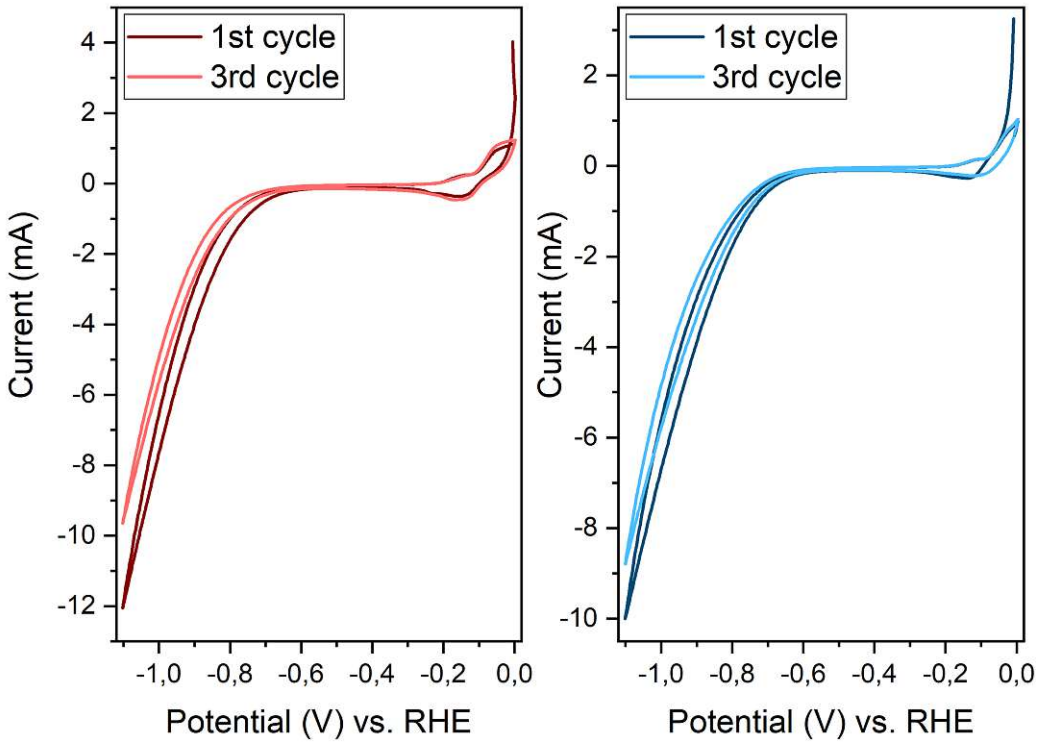

Figure 14 CV scans of In deposited Sn-plates with 55s deposition time from an opaque deposition solution under nitrogen (red) and carbon dioxide atmosphere (blue)

A 10s longer deposition time induced a change in the peak shape at lower potentials, with the peak separation appearing smaller in this sample. Additionally, it is notable that the reduction current under nitrogen exhibits a decreasing trend by the 3rd cycle with the 55s deposition time. Similarly, under carbon dioxide, the reduction current maintains the same decreasing trend.

BiOI deposited Sn plates

At first glance it is evident that the 1st cycle for both samples under nitrogen atmosphere revealed the nature of the reduction reaction of bismuth-oxide to metallic bismuth, which was also observed in the LSV measurements. This reaction is irreversible in the potential range of the CV-scans, and seemingly no residues of reducible species are left by the 3rd cycle of the CV-scans under CO_2 atmosphere.
In the case of the BiOI-deposited Sn-electrodes the peaks at lower potentials only appear in the reductive scan. The difference in the case of the BiOI sample is an even greater peak separation, meaning that a higher range of scanning potentials would have revealed the full oxidation peak with both sample under both atmospheres.
Furthermore, the sample with a 3-minute deposition time appears to have a smaller peak separation compared to the 2-minute deposition time sample.

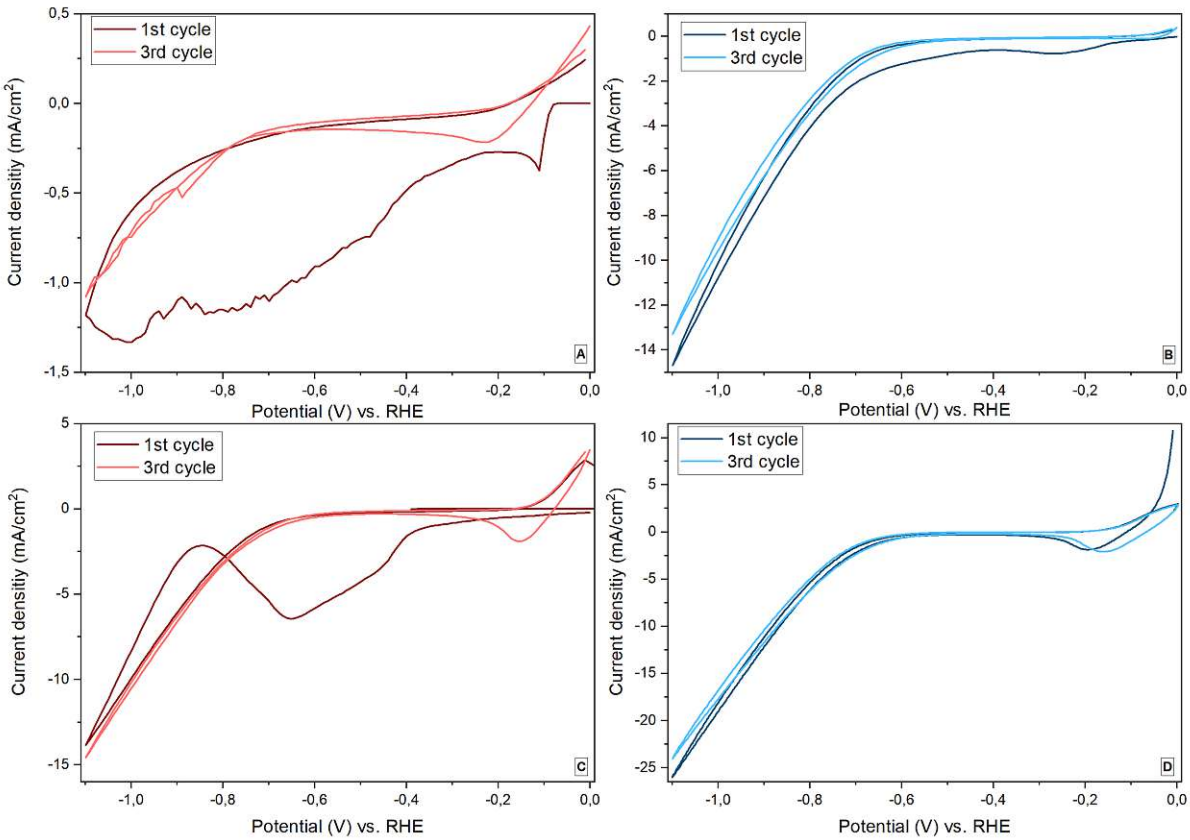

Figure 15 CV-scans of BiOI-deposited Sn-plates with 2min (A,B) and 3min (C, D) deposition times, under nitrogen (red) and carbon dioxide atmosphere (blue)

The reduction current both under nitrogen and carbon dioxide atmosphere seemed to be weakened by the 3rd cycle for both samples, with greater extent in the case of the 2min deposition time sample.

Metal-oxide dropcasted Sn plates

The CV scans of metal-oxide drop-casted Sn-plates closely resemble those of a blank Sn-plate, with one notable difference: during the reductive scan of the 1st cycle under a nitrogen atmosphere, only singular peaks are observed for both samples. However, after purging with carbon dioxide, a significant difference emerges. The peak at lower potentials almost disappears in the case of the In-oxide layer, while it remains observable in the case of Bi-oxide.

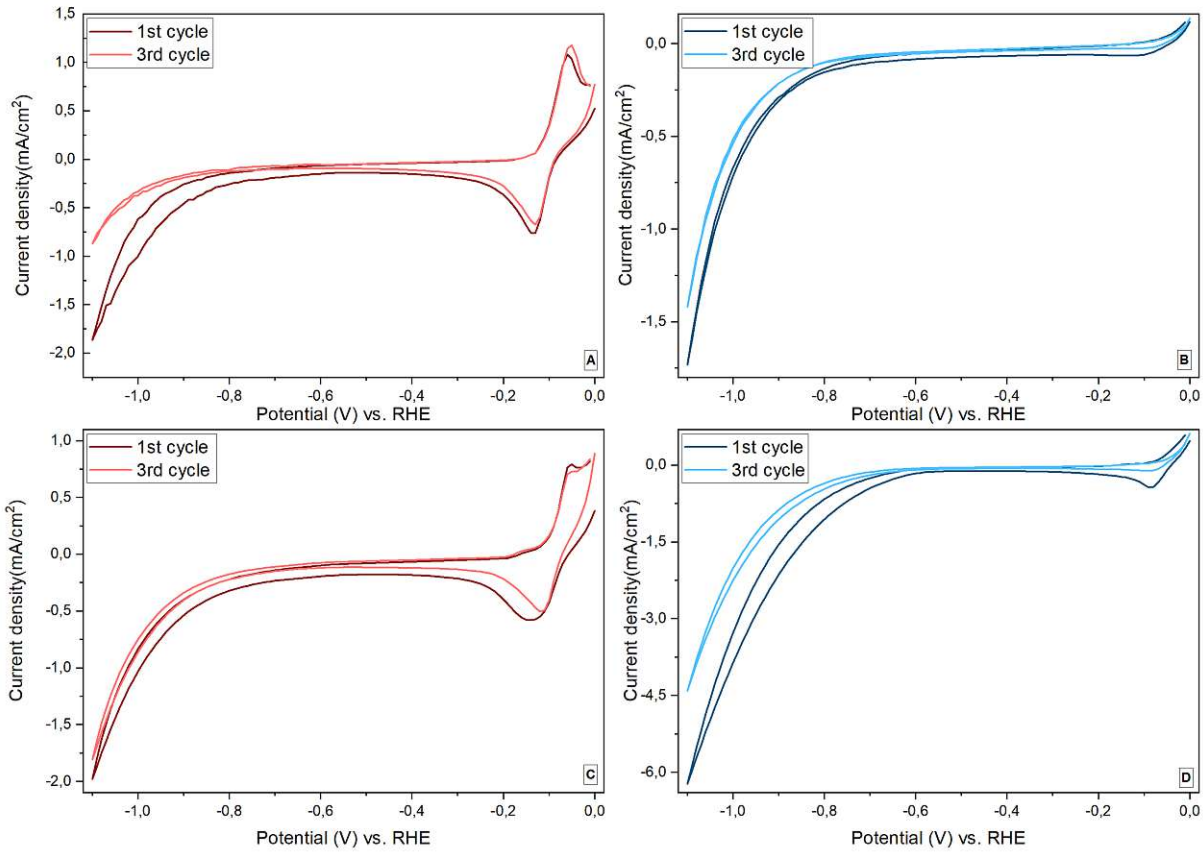

Figure 16 CV-scans of In-oxide (A, B) and Bi-oxide (C, D) drop-casted Sn-electrode under nitrogen (red) and carbon dioxide (blue) atmosphere

Unfortunately, the CV scans for these samples were conducted after the individual LSV measurements, meaning that oxides were likely fully reduced by the start of the CV cycles. However, based on the behavior of BiOI electrodes, it is also expected that any oxide layers would have been reduced during the first CV cycle under a nitrogen atmosphere in both cases. Notably, a difference in the shape of the reduction peaks of these oxide layers might have been observed in comparison to the LSV measurements.

Therefore, it can be confirmed that both types of electrodes after reduction exhibit electrochemical behavior similar to that of a blank Sn plate, with heightened current signals at the lowest scanning potential under nitrogen atmosphere.

Additionally, the reduction current with both samples under both atmospheres has taken up the decreasing trend by the 3rd scan of the measurement and the values are similar to the blank sample.

5.1.2. X-ray Diffraction

X-ray diffraction (XRD) is a technique used to analyse the crystalline structure of materials. By bombarding a sample with X-rays and measuring the resulting diffraction pattern, XRD provides information about the arrangement of atoms within the material, including crystal phase, crystallographic orientation, lattice parameters, and crystallite size. This technique is widely used in materials science, chemistry, and other fields to characterize the composition and structure of solids.

Sn- plate and Sn-deposited Sn-plates

X-ray scan of blank Sn-plate was performed to be able to distinguish the substrate from the deposited layers created during this thesis project.

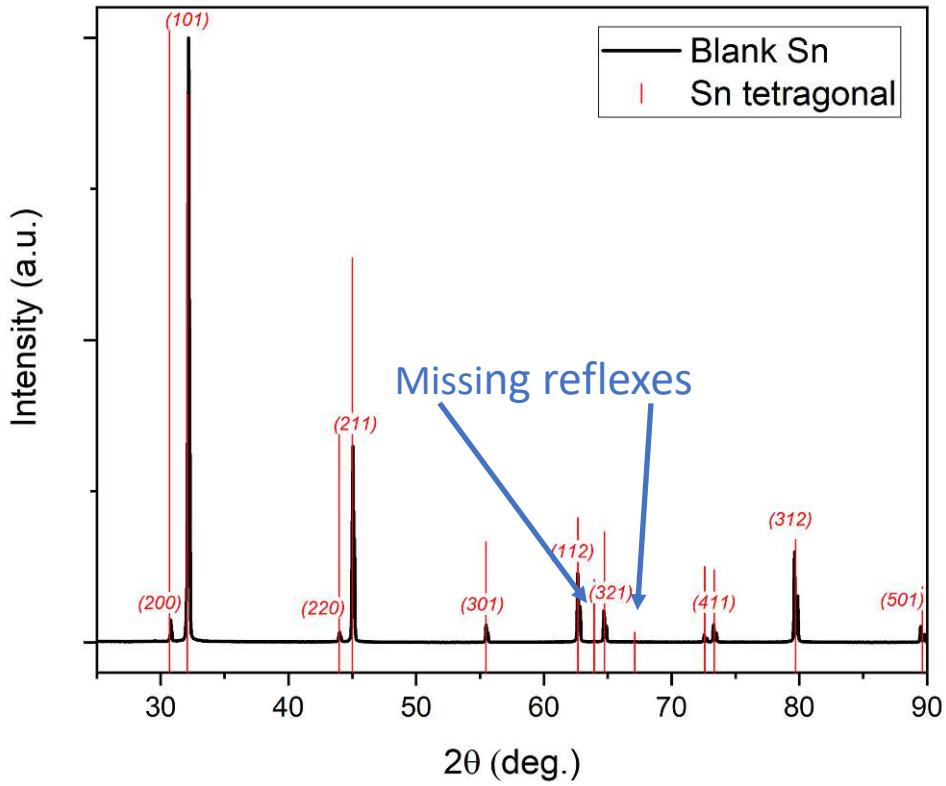

Figure 17 XRD pattern of a clean blank Sn-plate

Matching the diffraction pattern to reference it becomes evident that the Sn-plates are missing 2 of the reflexes (63.944- (400), 67.113-(202)) from the structure of a regular tetragonally coordinated lattice of Sn, the substrate is textured. The procedure of forming thin plates of metals can cause the crystals in the material to take up a preferred orientation that leads to a loss of certain reflexes, while making other reflexes appear more intense in the X-Ray diffraction pattern.

X-ray diffraction pattern of Sn-deposited Sn-plates reveal that the Sn-layer grown on the surface of the electrodes are also tetragonal, however the difference is that the intensity of

the reflexes at higher angles now appear to be more defined. This could be due to the fact that the lattice parameter c(Å) of the matched crystal structure to the deposited layer is smaller in comparison to what was matched with the blank sample's diffraction pattern or that the grown layer increased the volume of the sample, which leads to the number of reflexes of identical crystal planes to increase (multiplicity factor). Due to limited angular resolution Rietveld refinement was not possible to identify the exact ratio of the phase of the substrate and the phase of the deposited Sn-layers, as the lattice sizes are not significantly different leading to very small 2 theta shifts of the diffraction patterns.. The (400) reflex in this pattern is still missing, a possible explanation for that could be that the Sn-plate substrate acts as an epitaxial template for the Sn-layer to grow and therefore it also takes up the defects from the crystal structure. The rest of the peaks in the diffraction pattern belong to calcium carbonate from the material used to fix the Sn-plates to the sample holders. It shows up in the diffraction pattern, when the sample is too strongly pushed into the sample holder, causing the pastelin to spread out to the plane of the Sn-plate. The deposition time did not affect the crystal structure in any way, the same tetragonal phase was detected with both types of samples (1min and 1.5min deposition time) employed for the experiments.

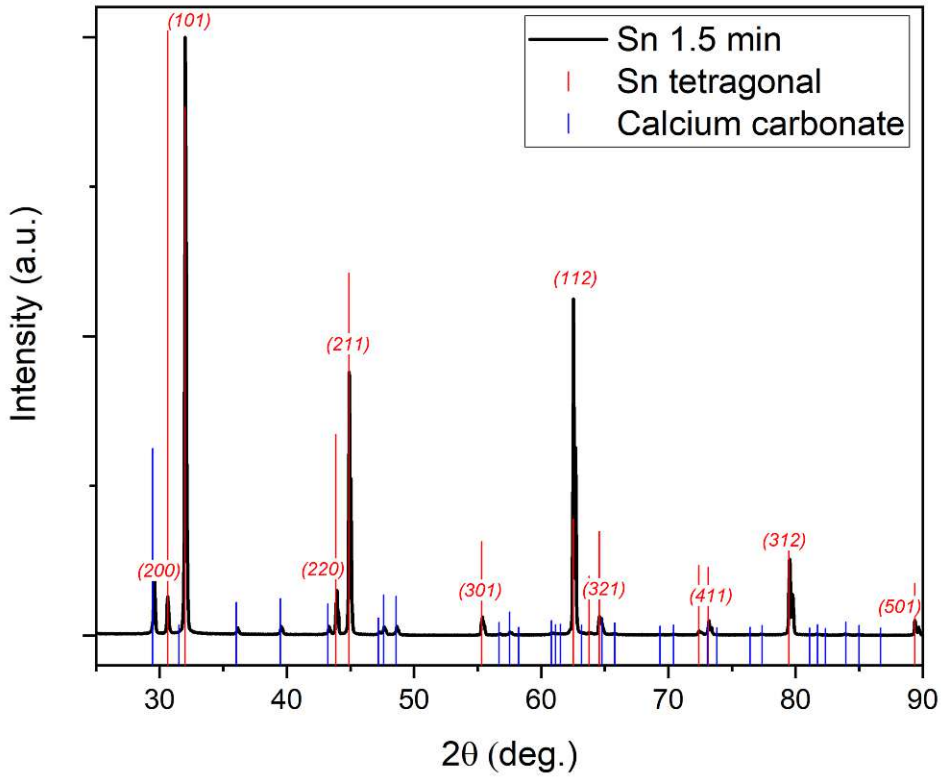

Figure 18 XRD pattern of a 1.5 min Sn-deposited Sn-plate

In deposited Sn-plates

For In-deposited Sn-plates it was theorized that the clear and opaque deposition solution possibly creates a difference in the crystal structure of the grown layer.

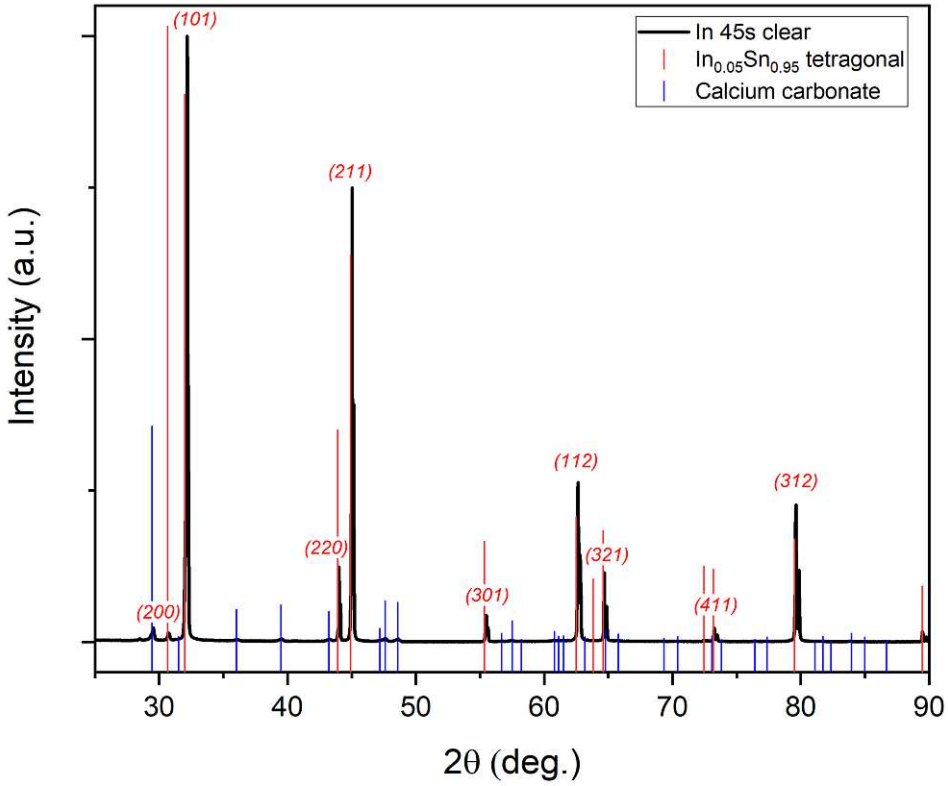

Figure 19 XRD pattern of a 45s In-deposited Sn-electrode using clear deposition solution

However, after evaluating the diffraction patterns for both samples with 45s deposition time it is evident that the same phase has formed in both cases. It appears to be that In rather goes into a tetragonally coordinated intermetallic compound with Sn under the electrodeposition conditions than forming a pure phase on the surface of the substrate.
Peaks at higher angle (64.620, 79.540) show up more and less intense in comparison to one another this again can possibly be due to the fact that the lattice parameters are slightly different, however it is still the same intermetallic compound.

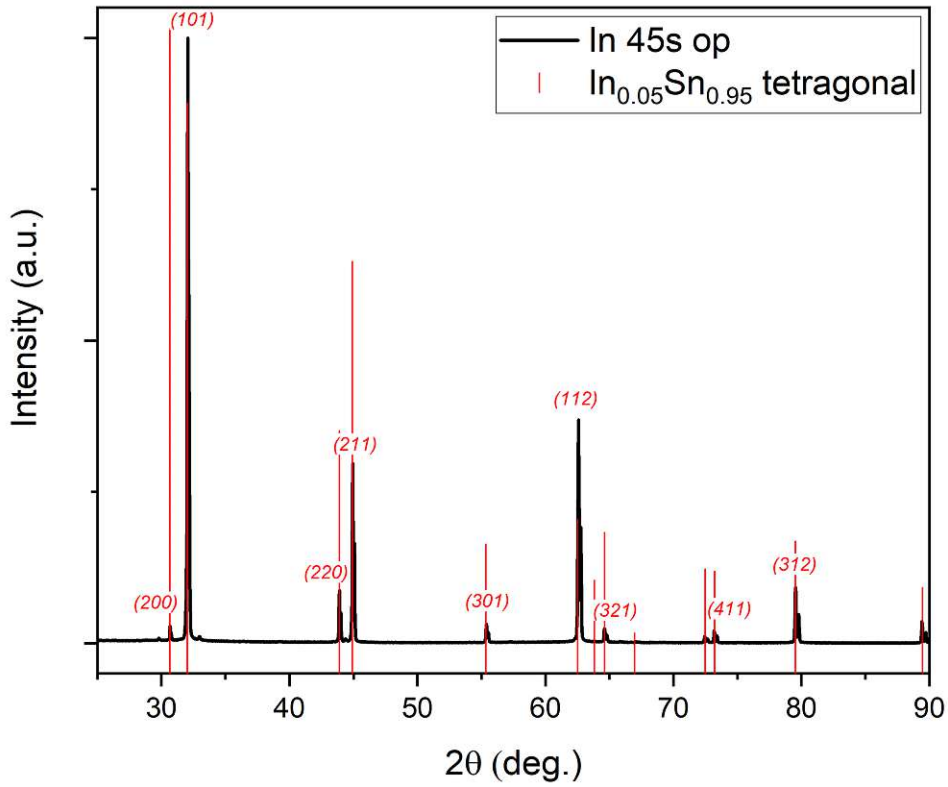

Figure 20 XRD pattern of a 45s In-depostied Sn-plate using the opaque deposition solution

Looking at the sample with 55s deposition time it is now evident that the longer deposition time still does not induce a single In-phase to be grown on the surface but rather another intermetallic compound with higher stoichiometric ratio of In in the crystal structure.
This formation of new compound also enables a new reflex (63.834) to appear in the diffraction pattern, that was considered to be lost due to the structure of the substrate. The peak intensities in this diffraction pattern do not appear to be that much different, as the lattice parameters are almost identical to the tetragonal structure of the sample with 45s deposition time from an opaque solution.

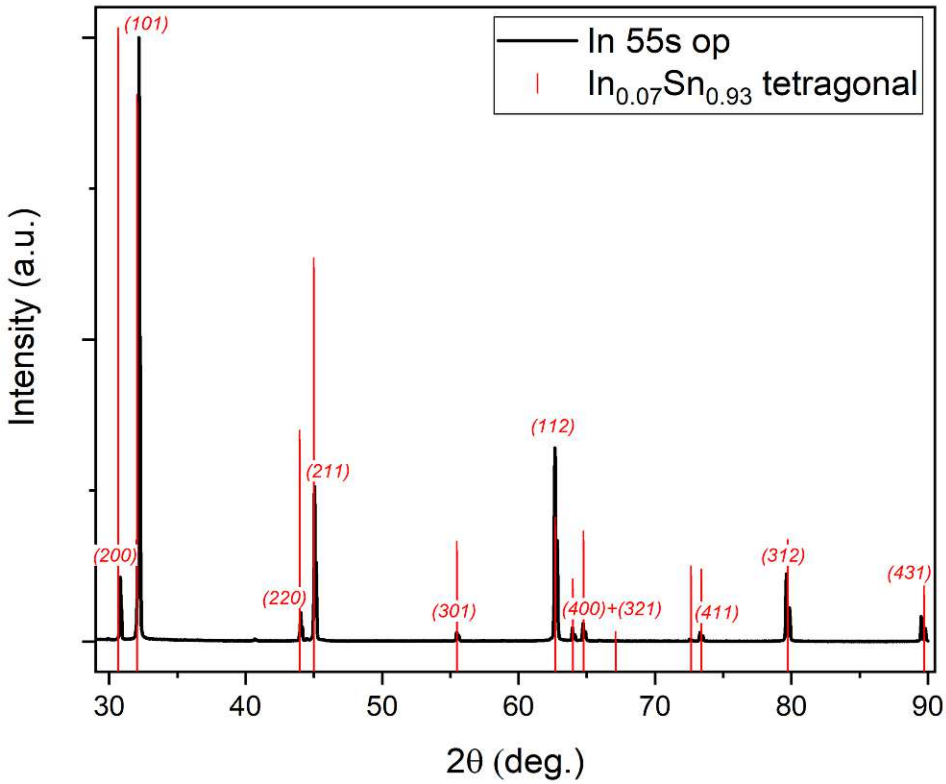

Figure 21 XRD pattern of 55s In-deposited Sn-electrode using the opaque deposition solution

BiOI deposited Sn-plates

BiOI deposited Sn-electrodes were created using the deposition method reported in a study for fabrication of $BiVO_4$ electrodes on FTO [5]. Changing the substrate did not affect the formation of BiOI on the Sn-plates, this was evident from the vibrant color of this compound on top of the electrode surface.

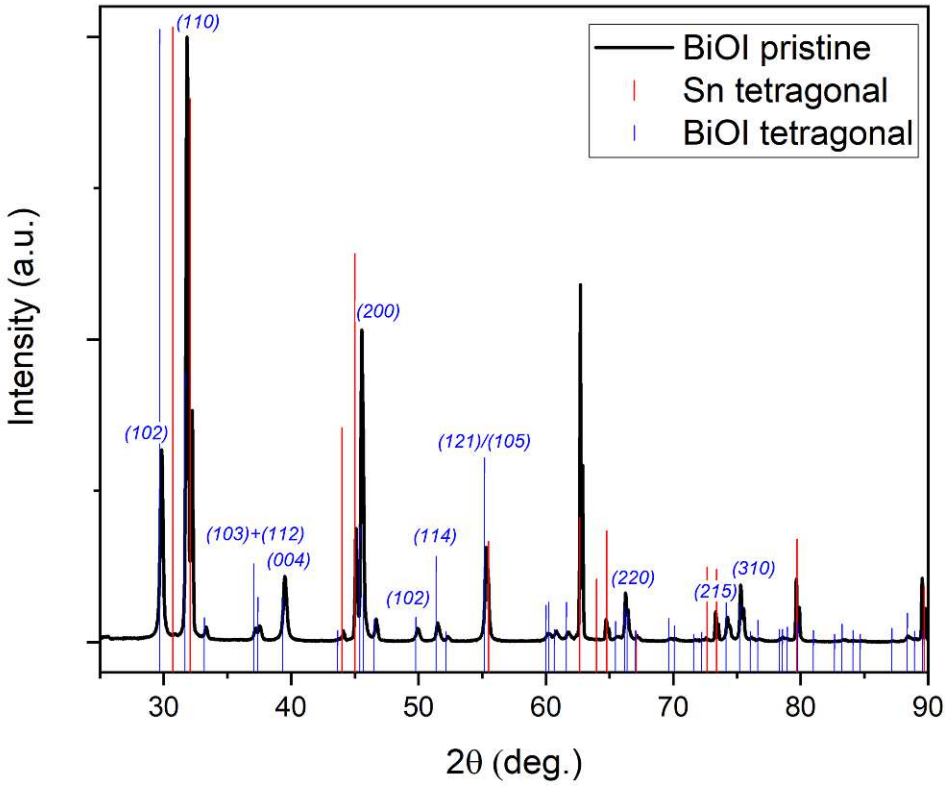

Figure 22 XRD pattern of a 2 min BiOI-deposited Sn-electrode as prepared

X-ray diffraction measurements also confirm a successful deposition of the desired layer, what is also obvious is that some reflexes are missing or appear broad from the pattern in comparison to the reference pattern, this could be due to the fact the layer grown on the surface is very thin and therefore the crystal structure suffer from constraints imposed by the substrate and strain effects. The sample volume penetrated by the X-ray is very small and the substrate underneath the thin layer may contribute to background signals or interfere with diffraction from the thin layer

BiOI-deposited electrodes were submerged in ca. 10ml of electrolyte overnight before each experiment, which turned the vibrant wine-red layer into a white-gray substance.

This layer later becomes black upon reduction during the electrolysis procedure.

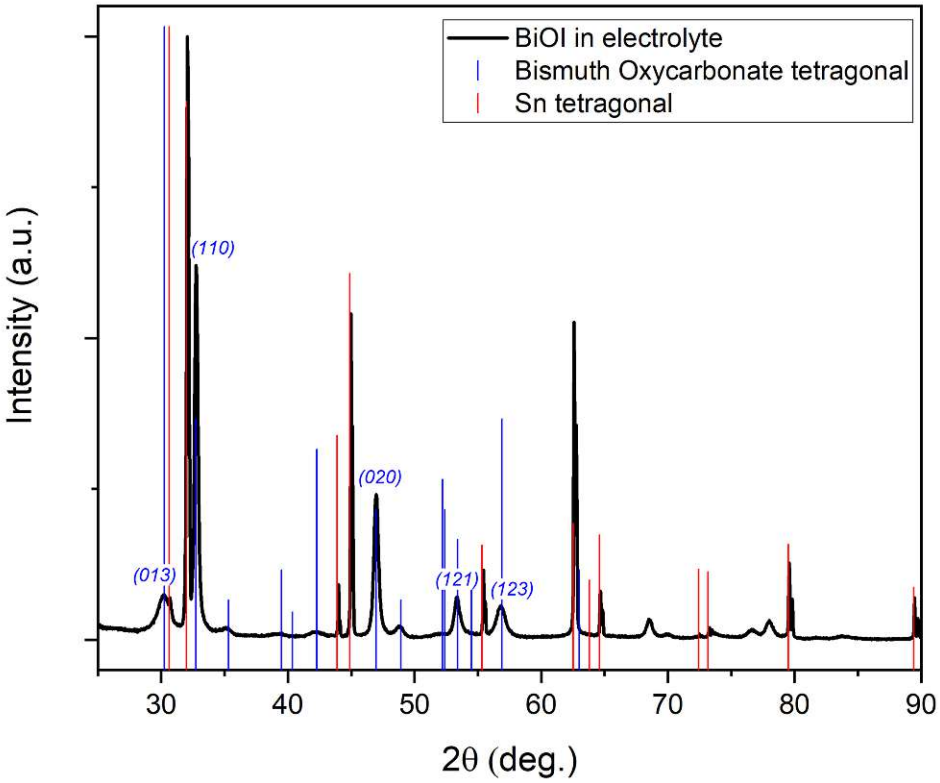

Figure 23 XRD-pattern of a 2 min BiOI-deposited Sn-electrode after dipping into 0.5M $KHCO_3$ electrolyte overnight

The submerged electrodes appear to form bismuth subcarbonate or bismuth oxycarbonate after interaction with aqueous 0.5M $KHCO_3$. Apart from the newly formed carbonate, residues of the BiOI peaks are still detectable.

Metal-oxides

Indium and Bismuth-oxide were synthesized using microwave reactor, X-ray diffraction pattern of the Bi-oxide powder as synthesized confirms that the compound was successfully formed. Reference patterns of possible impurities stemming from the precursors do not align with the remaining unmatched peaks from the diffraction pattern of the sample. Therefore, the remaining reflexes possibly could be allocated to impurities detected on the sample holder used in the measurement. However, the fact that the majority of the pattern aligns with the desired compound experiments were conducted using the powder. Since the electrolysis involves reducing potentials, it is also expected that the oxide powder or any other Bi-compound will be partially reduced to metallic Bi in the process.

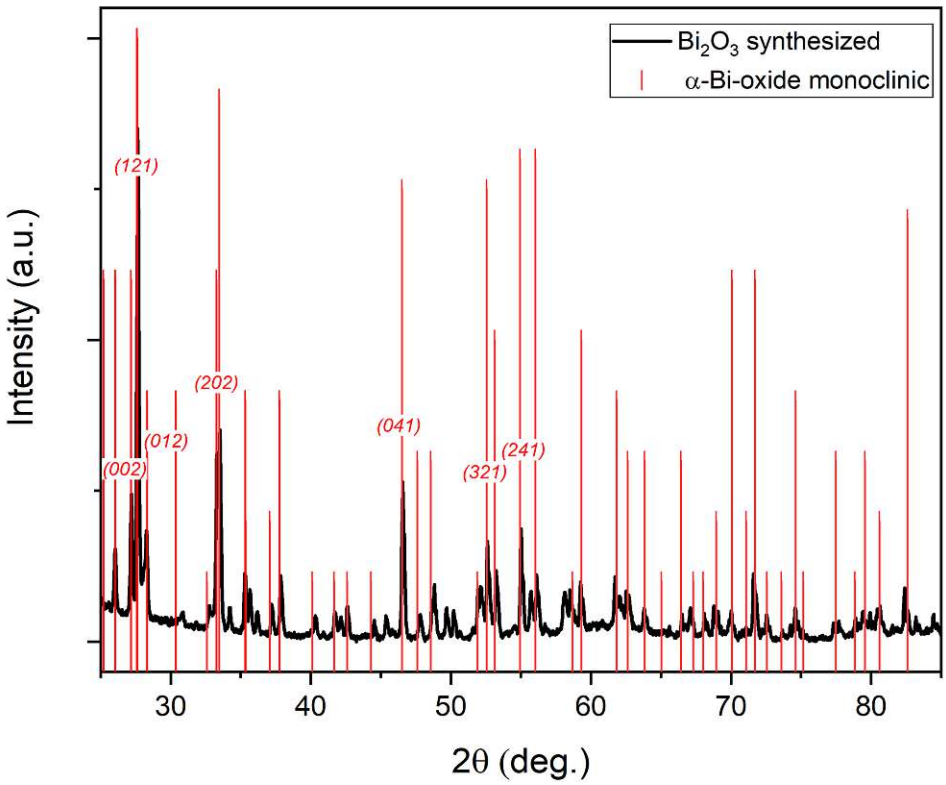

Figure 24 XRD pattern of the Bi-oxide powder as synthesized

X-ray diffraction of the In-oxide powder reveals that the product is indeed at least amorphous, but possibly also consists of nanoparticles. The diffraction pattern of the sample contains broadened peaks that are impossible to match, hence this section does not contain any record of this measurement.

5.1.3. In_2O_3-powder characterization

Dealing with amorphous In-oxide or In-oxide nanoparticles has pressed the need of exploring other ways to characterize the synthesized product to confirm the reaction was successful. Records of FT-IR measurements of the material [32],[33] has confirmed the possibility to identify and characterize In_2O_3 as synthesized.

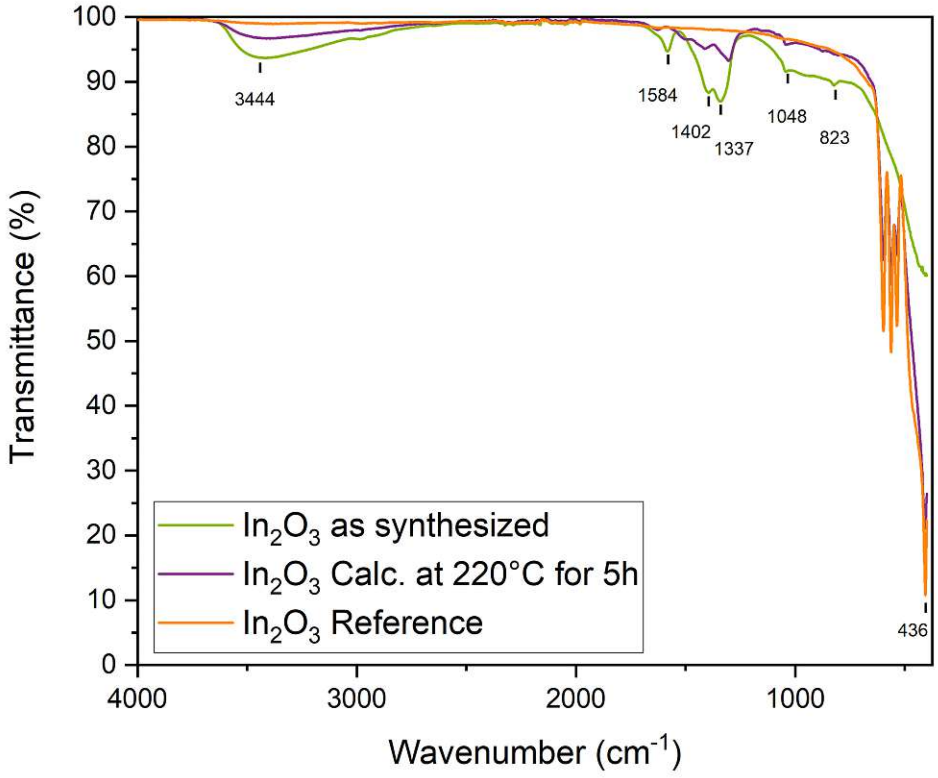

Figure 25 FT-IR spectra of In-oxide powder as synthesize, calcinated and reference

On the first glance characteristic peaks (3444 cm^{-1}, 1584 cm^{-1}) for O-H-bond stretching and bending vibrations can be identified in the spectra of the as synthesized powder, these peaks are possibly caused by residual water from non-sufficient drying or a side product of the reaction $In(OH)_3$ for instance. Other smaller peaks according to literature can be allocated to deformed vibration absorption of In-OH bond, 1048 cm^{-1} and 823 cm^{-1} which further supports the formation of the side product. The strong absorption peak at 436 cm^{-1} corresponds to characteristic phonon vibration of cubic In_2O_3[32],[33] . Two stronger absorption bands in the fingerprint region in the spectra are suspected to belong to the educt used in the synthesis of this powder, hexamethylenetetramine. Absorption bands in the region 1180-1360 cm^{-1} are identified as secondary amine C-N-C assymetric stretching bands, while in the same region alkane, mainly methyl, C-H bond stretching and bending are also characteristic, which lines up well with the structure of the heterocyclic compound[34]. Calcinating the synthesized powder made the absorption bands of O-H bonds and other impurities weaker, which concluded the effectiveness of temperature treatment. Considering that the absorption bands of the unwanted species significantly weakened the calcinated powder was later used for ink preparation to fabricate In-oxide- Sn electrodes.

5.1.4. Scanning electron microscopy and Energy dispersive X-ray Spectrometry of pristine metal-oxide Sn-electrodes (SEM and EDX)

SEM images were recorded of the pristine drop-casted electrodes, and EDX measurements were also performed to further confirm the composition of the metal-oxide powders.

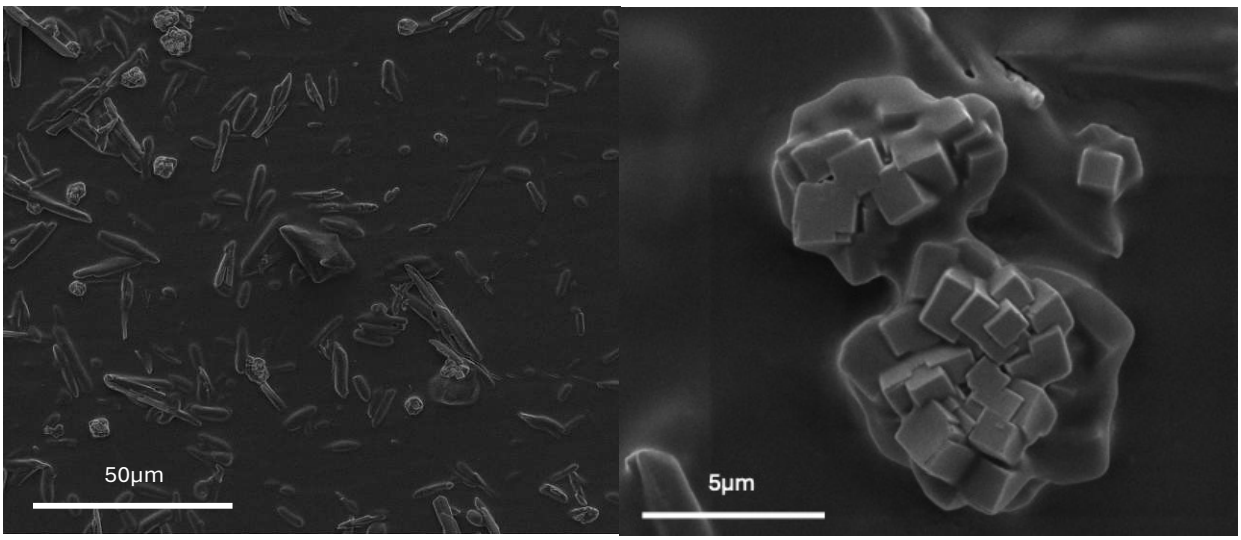

Figure 26 SEM images of Bi-oxide drop-casted Sn-electrode at 2000x and 30000x magnification

On first glance, the surface of the electrode at lower magnification looks evenly coated with the Bi-oxide crystallites, this image also reveals the diversity of crystal shapes of the monoclinic structure. Some appear rod-like and some appear as cluster of smaller cubes portrayed on the image with 5µm magnification.
The edges and corners of the crystallites rather look smooth and slightly less defined, this is due to the resin binder, added to the drop-casting ink, coating the crystals.

Table 4 List of elements and their atomic and weight percentage found in the EDX measurements of each indicated areas of the Bi-oxide Sn-electrode

Element	Cluster		Rod-like crystallite		Substrate	
	Atomic %	Weight %	Atomic %	Weight %	Atomic %	Weight %
C (K)	28.1	5.9	30.4	6.9	18.4	4.2
O (K)	23.7	6.6	17.3	5.2	2.2	0.7
F (K)	25.6	8.5	31.7	11.4	43.2	15.7
S (K)	0.8	0.5	1.0	0.6	1.8	1.1
Bi (M)	21.3	77.5	18.7	74.1	-	-
Sn (L)	0.5	1.1	0.8	1.8	34.5	78.3

EDX measurement revealed the composition of both type of crystallites to be Bi-oxide, with similar ratio of bismuth and oxygen. Furthermore in the spectrum sulfur, fluorine and carbon was also detected, these elements are present from the resin binder Nafion/ Aquivion used in the preparation of the electrodes. Scan of the areas where no visible crystallites were seen were used to confirm the successful identification of Bi-oxide on the Sn-plate as the Sn content has a stark difference between areas of both types of crystals and the Sn-plate itself with resin on top.

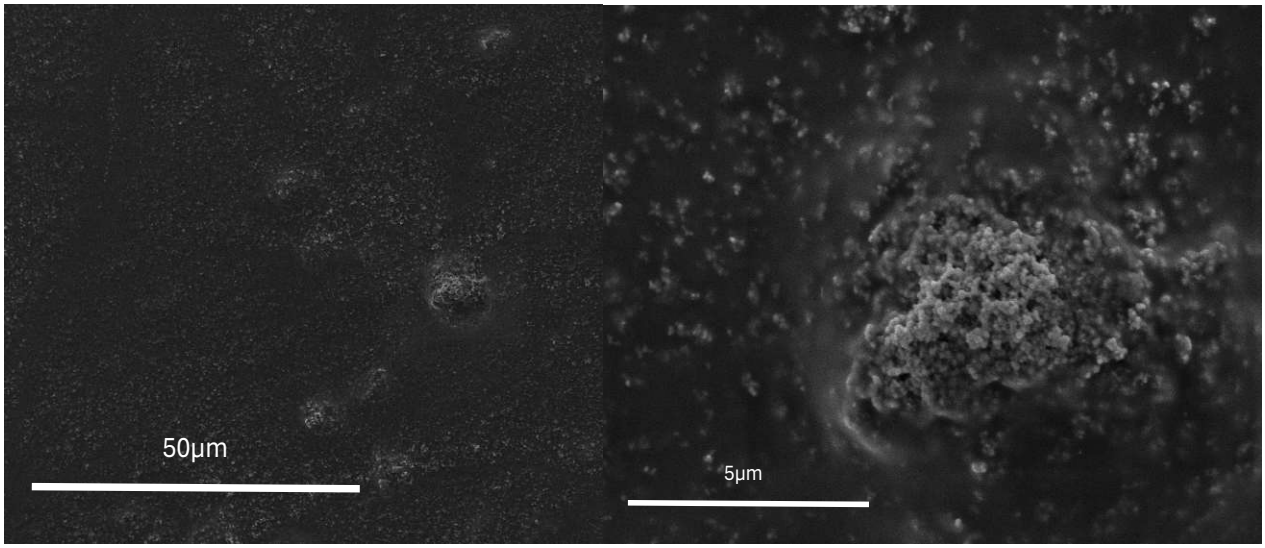

Figure 27 SEM images of Bi-oxide drop-casted Sn-electrode at 2500x and 20000x magnification

In the case of In-oxide drop casted electrodes, it is evident that the particles are much smaller, and are more densely distributed over the surface with some amount of bigger clusters scattered. On higher magnification it can be also concluded that the material consists of nanoparticles even after calcination, and appears in spherical shape. These findings support the hypothesis of nanoparticle In-oxide.

Table 5 List of elements and their atomic and weight percentage found in the EDX measurements of each indicated areas of the In-oxide Sn. electrode

Element	Cluster		Substrate	
	Atomic %	Weight %	Atomic %	Weight %
C (K)	23.4	6.9	20.4	4.8
O (K)	18.3	7.3	3.7	1.2
F (K)	32.3	15.2	39.6	14.6
S (K)	1.7	1.3	2.3	1.4
In (L)	22.6	64.3	4.4	9.9
Sn (L)	1.7	5.0	29.6	68.2

Results from EDX measurement confirm the particles to be In-oxide, carbon content of both areas are very similar to the areas of Bi-oxide Sn-electrodes, which also leads to the conclusion that the amount impurities found in the FT-IR measurerent is supposedly very low, it does not interfere with the catalysis. Measurement of an area where only the Sn-substrate is expected also contains smaller amounts of indium, which further points to the small size of the particles and the dense distribution of them.

5.2. Catalytic Performance testing

5.2.1. Electrocatalytic CO_2RR

Electrocatalytic CO_2 reduction reaction (CO_2RR) involves the conversion of carbon dioxide (CO_2) into value-added products such as formic acid using electrical energy and the bimetallic catalysts.
This section aims to present the results expressed in Faraday efficiency for the initial testing experiments as well as the values at 3 different applied potentials for each type of samples, these values are derived from series of 3 experiment at each potential.

Sn deposited Sn-electrodes

The initial testing served as a way to find out how the layer thickness affects the reactivity of the surface to produce formate. These experiments were done only at the highest potential used through this research, -1V vs. RHE for 1h.

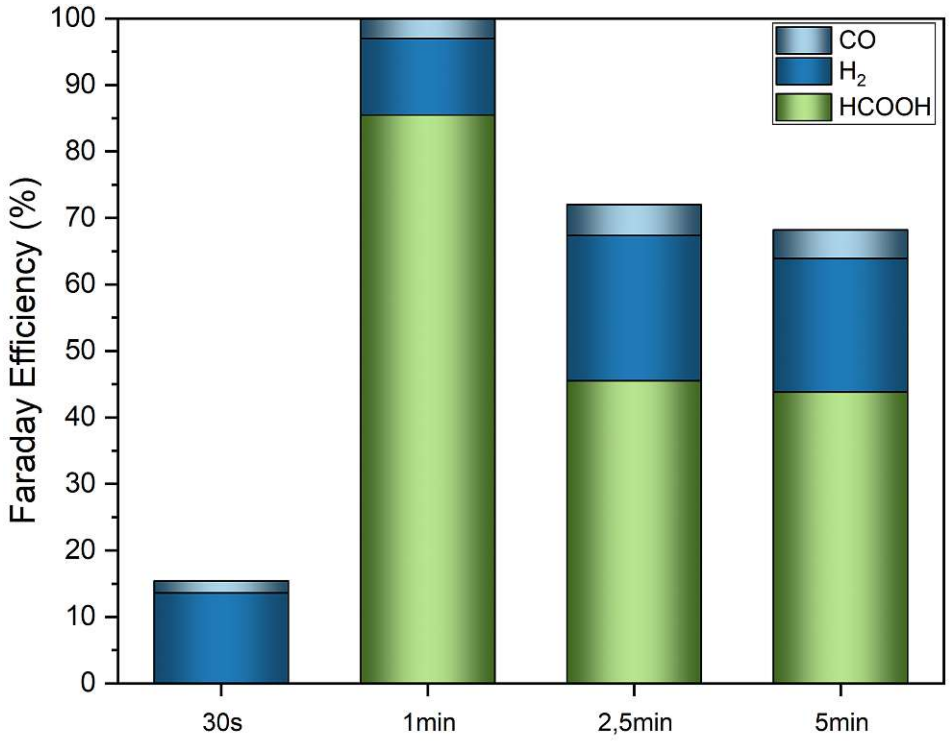

Figure 28 FE values of various products formed during CO_2RR using Sn-deposited Sn-electrodes with different deposition times

At first glance it becomes obvious that 30s deposition time sample did not deliver any formate, this occurrence is in a way not expected as a simple blank Sn-plate still performs considerably good at these conditions. Furthermore, the sample with 1min deposition time reached a Faraday efficiency of almost 90% which gave the choice of having one type of sample with 1min deposition time. Since the longer deposition times seemed to have a drawback on the efficiency values the second choice became 1.5min deposition time, as the reason is uncertain, why the sample with 30s deposition time did not produce any formic acid and with the electrodeposition set-up it was also difficult to achieve shorter time windows in a controllable manner.
Experiments with blank Sn-plate were done in the same series of 3 experiments to be able to compare the performance of the different type of electrodes prepared for this thesis research.

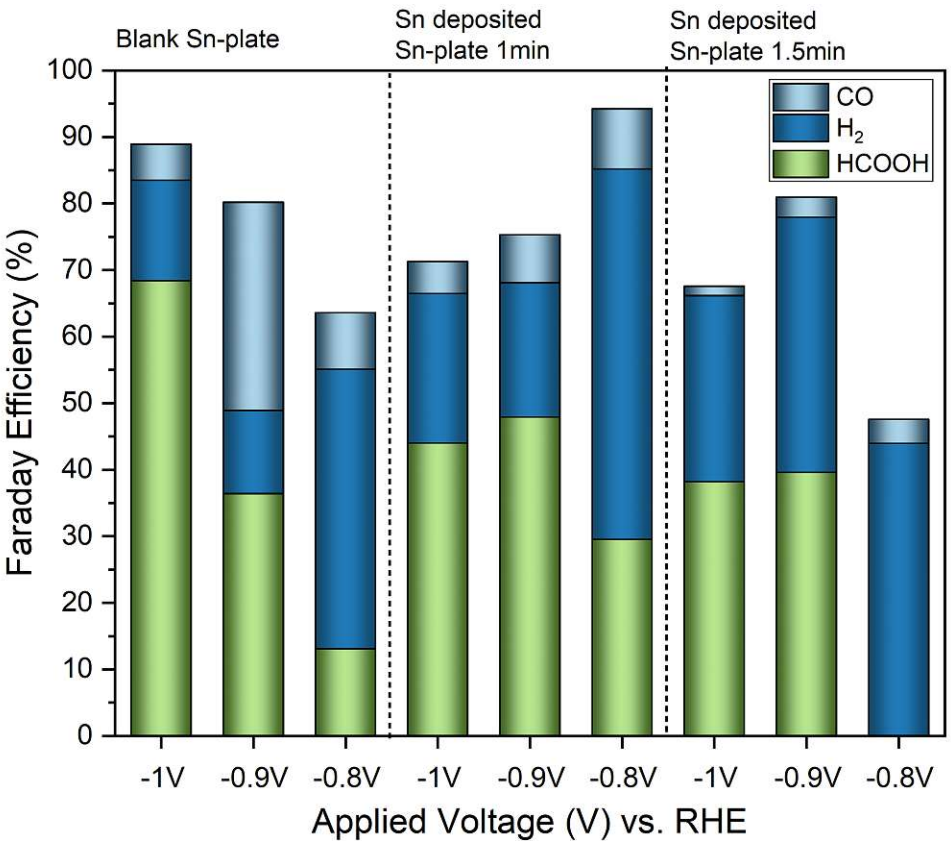

Figure 29 FE values of various products formed during CO_2RR using Sn-deposited Sn-electrodes with different deposition times compared with the performance of blank Sn-electrodes

Comparing the results with the blank experiments it is evident this time that the pure Sn-layer on the surface did not contribute to a better catalytic performance at -1V vs. RHE of the electrodes. However, at lowered applied potentials in the case of 1 min deposition time an improvement in formic acid production can be observed, but it also comes with the cost of heightened HER activities. Furthermore, the sample with 1min deposition time did not deliver the same results over the 3 experiments at -1V vs. RHE as it did during the initial testing. Comparing the 1.5min and 1min deposition time sample together it is evident that the 1min sample performed better at all applied potentials. Overall, the performance of the blank sample appears to be the outstanding and also the competing HER reaction with this electrode is rather minimized.

Overall it is also evident that the thicker the deposited Sn-layer presumably get via longer deposition times, the lower the amount of formate can be produced at the same applied potentials.

Another key point is that the experiment results do not add up to a 100% Faraday efficiency value which point toward the possibility of the formation of other CO_2-reduction products such as methanol or even ethanol, however the concentration of these products are possibly so low that it is not detectable with any of the methods employed for this thesis research. On the not so optimistic side, another occurrence surely contributing to less than 100% FE is morphological changes of the surface of the electrode. As it was observed during the electrochemical characterization, the electrode undergoes changes which also take up electrons in the process, which also lead to less electrons consumed for product formation during the experiments.

In literature the FE values go up to as high as 91% for formic acid, in 0.1M $KHCO_3$ electrolyte at -1.4 vs. SCE which approximately corresponds to -0.72V vs. RHE [22]. However in this work, Sn was deposited on top of Cu-foil, and the paper also points out that the Sn-layer does not proportionally grow thicker with the increased current density during the electrodeposition and it is thinner than expected, hence it as arguable that the improved catalyst activity is due to the interaction of Cu with Sn. Other reports of bulk Sn-electrodes for formate production point out the dependence of a native oxide layer on the surface, which enhances the selectivity and performance of the metal. One of these reports 84% FE with an untreated bare Sn-electrode (99.99%, 0.5mm thick, 1cm^2) which was not reached with any of the blank nor deposited electrodes used in this research[19]. In another paper the value with untreated Sn-plate has reached 91% in 0.1M $KHCO_3$ at -1.8V vs Ag/AgCl which approximately corresponds to 1.1V vs RHE, however details of their working electrode is not revealed in the work[23], therefore it is plausible that some amount of native oxide layer on the surface played a significant role in the increased efficiency.

In-deposited Sn-plates

In-deposited Sn-plates were also tested with different deposition times, in this case the maximum deposition time achieved was 1.25min, any electrodeposition experiment longer than that resulted in the In-layer falling off the plate once the current flow stopped. The initial experiments were done again at an applied potential of -1V vs RHE for 1h.

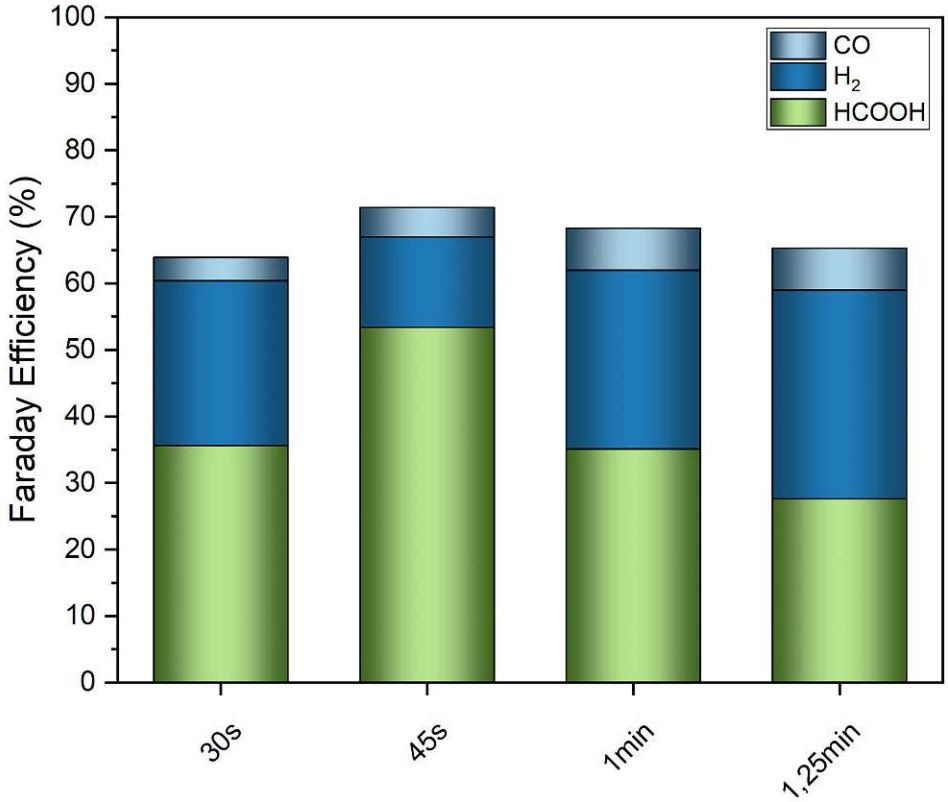

Figure 30 FE values of various products formed during CO_2RR using In-deposited Sn-electrodes with different deposition times

The testing concluded that the sample with 45s deposition time appears to deliver the best results out of all. This became therefore one of the chosen deposition time to proceed with,

the second time window then was chosen to be 55s on the basis that it is still closer to 45s and the optimum layer for better catalytic performance was assumed to be in that range.
Following the initial testing and the sample preparation for the series of experiment the different types of samples were put through the same electrolysis procedures as the Sn deposited Sn-plates.

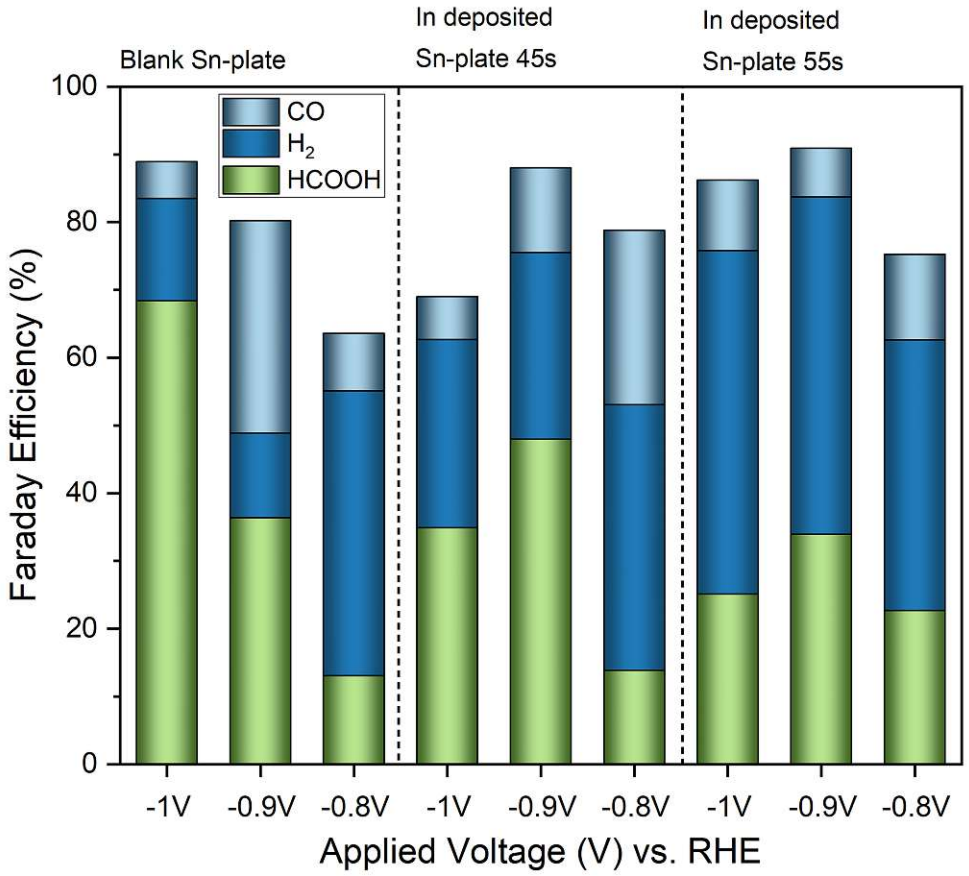

Figure 31 FE values of various products formed during CO_2RR using In-deposited Sn-electrodes with different deposition times compared with the performance of blank Sn-electrodes

These results conclude that incorporating a secondary metal into the Sn-plate can potentially lower the overpotential for CO_2-reduction to formate. While these experiments did not deliver higher efficiency values at -1V vs. RHE it is evident that the In-deposited Sn-plate electrodes perform better at -0.9V and -0.8V vs. RHE in general than the blank sample.
Overall, all samples appear to have a trend of higher Faraday efficiencies at -0.9V vs. RHE. Both electrode types,with deposition times of 45 seconds and 55 seconds, showed increased CO production at -0.8 V. Notably, the sample with a deposition time of 55 seconds performed the worst, yielding very low formic acid levels while hydrogen evolution dominated as the primary competing reaction.
It is also case here as with the Sn-deposited electrodes that the FE values do not come up to 100%, here however, there are firm indicators of other liquid product, such as methanol, forming during the electrolysis, the signals in the NMR-spectra are regrettably very low, hence the results are not indicated in Figure 29. In Section 9. of this work, Figure 36. aims to provide records of these signal appearances.

In the work of Hori a Faradaic efficiency value of 94.9% for formic acid on pure In electrode was reported, for this research the authors used 0.1M $KHCO_3$ at -1.55V vs NHE, which converts

to approximately -1.1V vs RHE overpotential[11]. In another work indium tin oxide (ITO) nanobranches were fabricated on Cu foil substrate, these electrodes were then reduced to bimetallic alloys. The highest FE efficiency, 78.6%, was reached at -1.1V vs RHE in 0.1M $KHCO_3$. This value was outperformed by simple In-film deposited on the same substrate in the frame of the same work, formic acid FE value with the mentioned electrode at the same potential reached 92.3%[24]. Although the electrodes fabricated in this work did not surpass the reported values in literature, they operated at significantly lower applied potentials. Notably, all electrodes showed better selectivity and activity for formic acid production at the lower potential of -0.9 V, 49,94% with 45s deposition time electrodes.

BiOI-depsotied Sn-plates

Due to the ease of time control with the BiOI-deposition method a wider variety of samples were prepared for the initial testing for Bi-Sn-electrodes.

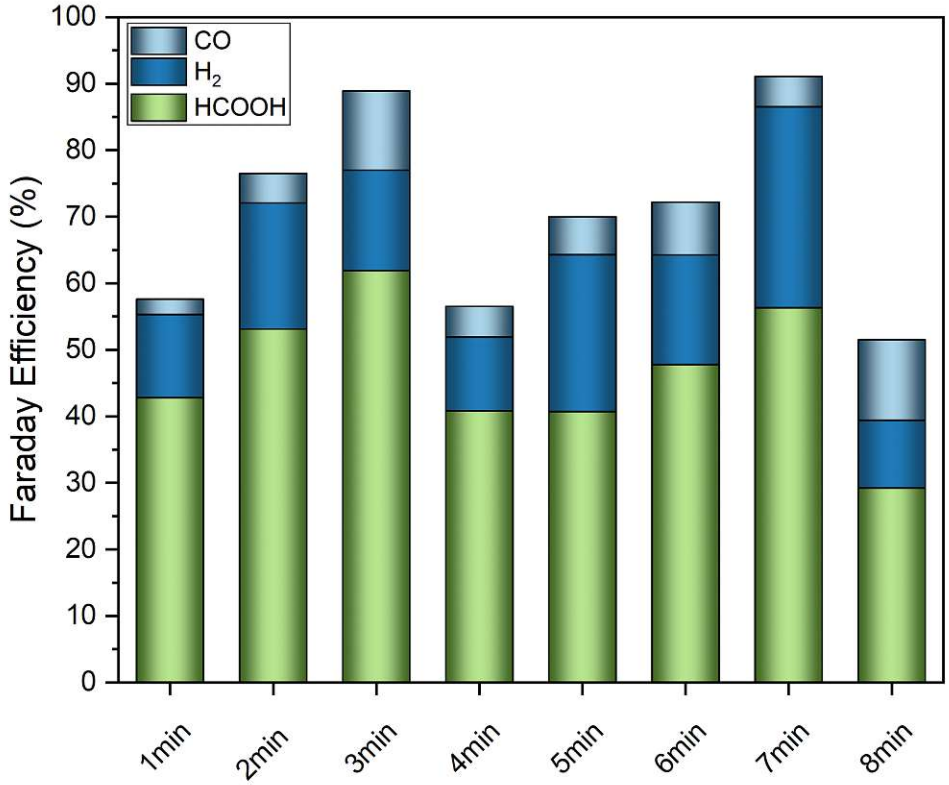

Figure 32 FE values of various products formed during CO_2RR using BiOI-deposited Sn-electrodes with different deposition times

After evaluating all the experiment results in this series, the conclusion was to work further on with the samples of 2 and 3min deposition times. The sample with 7min deposition time is considered to be outlier as the transferred charge during the deposition appeared to be equal amount as it was in the case of a 3min electrodeposition. This means that the BiOI layer on the Sn-plate contains the same amount of the species as their 3min counterpart.

Moving on to the series of 3 different applied potentials with the now only 2 types of samples shows that the electrodes with 2min deposition time produced overall more formate during the electrolysis than the samples with 3min deposition time. In comparison to the blank

experiments the same observation can be made, that these electrodes collectively deliver more formate with lower applied potentials than the Sn-plate itself.

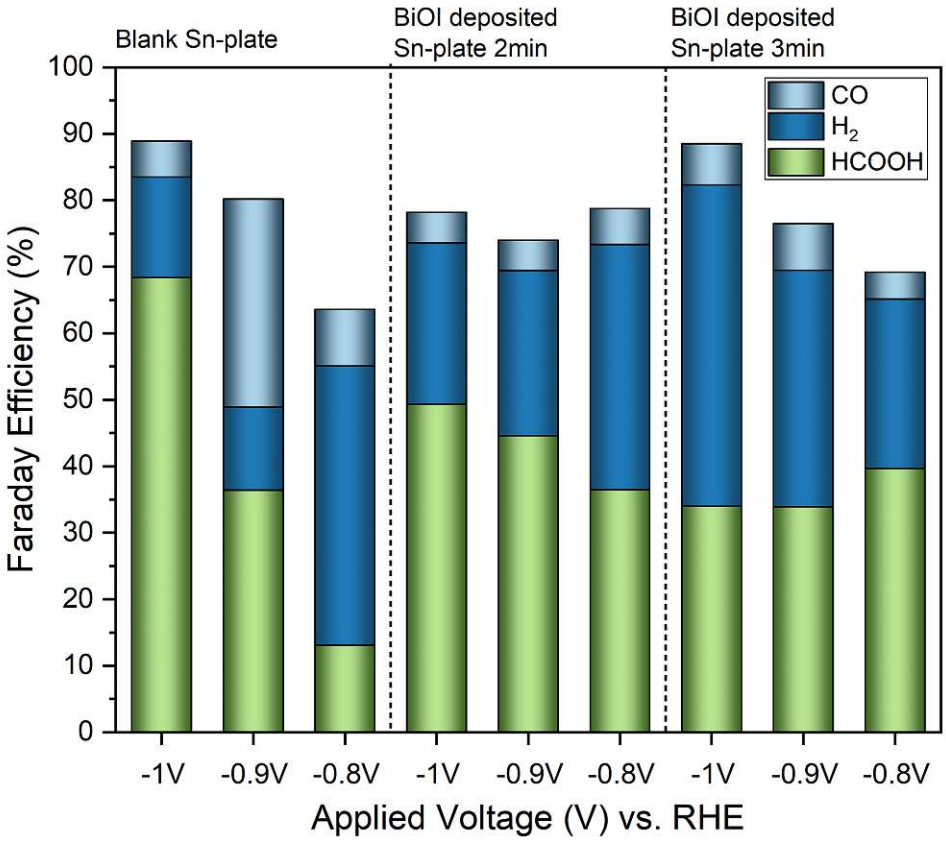

Figure 33 FE values of various products formed during CO_2RR using BiOI-deposited Sn-electrodes with different deposition times compared with the performance of blank Sn-electrodes

On the other hand, a slightly growing trend of formate with decreasing applied potential is also notable with the sample with 3min deposition time, which is not the case with the samples with 2min deposition time.

Due to the reducing potentials and redox reactions observed in the electrochemical characterization of these electrodes, it is evident that a portion of electrons was consumed in structural and compositional changes at the electrode surface. As a result, the Faradaic efficiency (FE) values do not add up to 100%. On a positive note, liquid samples from experiments with BiOI-deposited Sn electrodes also catalyzed the formation of other liquid products, likely methanol. This occurrence is similarly documented in Section 9, as with the experiments involving In-deposited electrodes.

In literature scientists have created a 2D-architecture out of BiOI using liquid precipitation method and surfactant for templating. The structure was then annealed to remove the surfactant and the BiOI was reduced to metallic Bi nanotubes via in-situ electroreduction. The maximum FE for formate lies at 97.1% using their annealed Bi-nanotubes at -0.9V vs. RHE[25]. While the in-situ Bi-Sn electrode fabricated in this work performed with maximum 49.33% FE at higher applied potential, which points out that nanostructures and more sophisticated surface architecture of a catalyst will enhance its performance due to the increased active sites.

In another study scientists have created Bi-Sn bimetallic catalyst on carbon fabric substrate. These electrodes were made by depositing SnO_2-nanosheet hydrothermally onto the substrate

which was followed by electrodeposition of Bi-nanoparticles on top of the nanosheets. The substrate served as a support for the nanosheets to grow vertically without the usage of polymer binders. These electrodes were then pre-reduced to Sn-Bi alloy in situ at constant -1.14V vs. RHE before catalytic testing. Their study revealed that the oxide derived Sn-Bi bimetallc catalysts can produce formate with up to 94% FE at -1.14V vs. RHE in 0.5M $KHCO_3$ electrolyte[25]. In another study Bi-Sn alloy with different stochiometric compositions were created using electrodeposition on Cu-mesh substrate, here Sn was deposited on top of Bi, the morphology resembles a velvet-network. The catalytic testing revealed a maximum FE of 94.8% for formate production with a Bi_5Sn_{60} electrode at -1V vs. RHE in 0.1M $KHCO_3$ electrolyte[28].

BiOI electrodeposited Sn-plates after electrocatalysis

Since the electrode preparation strategy was to create in situ Bi-layer on top of the Sn-plates for this series of experiments an additional XRD scan was done after the electrocatalysis, to investigate how the surface has changed during the experiment.

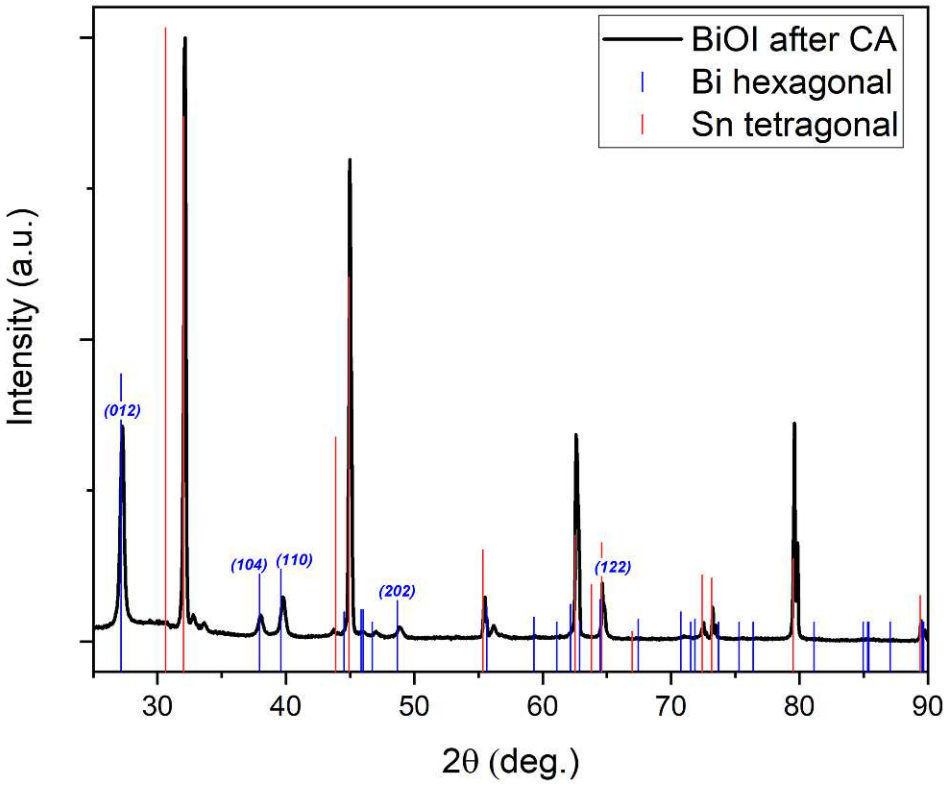

Figure 34 XRD pattern of BiOI-deposited Sn-electrode after electrolysis

Matching the XRD scan with reference patterns, the same tetragonal Sn-phase could be allocated to some of the characteristic reflexes. However, as it was observed before some of the reflexes are missing from the tin plate, due to the production method, which was discussed in previous sections. A second phase was identified as a hexagonal pure metallic Bi-phase. These reflexes appear in the pattern not so well defined as the ones paired with the tetragonal Sn-phase, this is most likely due to the fact that the layer is thin and the bulk Sn-substrate creates background interference the same way as discussed with the BiOI layer in *Section 5.1.2*.

Metal-oxide dropcasted Sn-electrodes

Metal-oxide dropcasted Sn-electrodes were prepared for the purpose of ensuring even load of secondary metal species on the Sn-plates and hence mitigate the issue of non-reproducibility that occurred throughout the previous series of samples.
For this series of experiments no initial testing for different concentrations were done, the synthesized powders were dispersed in IPA with 10mg catalyst/ ml solvent concentration with the addition of Nafion to ensure that the applied layer on the Sn-plate stays intact once it is submerged in the electrolyte for electrolysis.

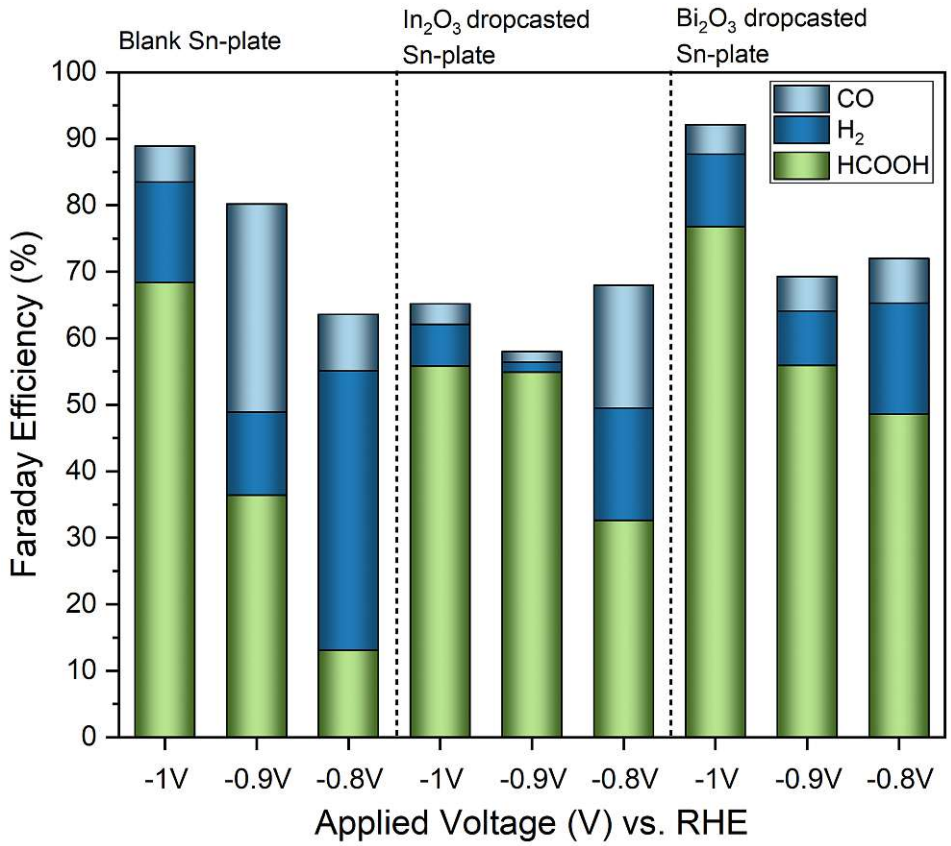

Figure 35 FE values of various products formed during CO_2RR using Bi- and In-oxide drop-casted Sn-electrodes compared with the performance of blank Sn-electrodes

At first glance it becomes evident that both types of electrodes have increased the formate production at lower applied potentials in comparison to the blank samples. While In-oxide did not outperform a simple Sn-plate at -1V vs. RHE, Bi-oxide did deliver higher amount of formate overall.
On the contrary to the electrodeposited electrodes it is also clear that the trend of increased formate production at -0.9V vs. RHE applied potentials is not observable anymore.
None of the series of experiments have reached 100% total Faraday efficiency in this series, which means that there is a possibility of other products also forming with this type of samples as well. However, due to the higher number of electrons required to be transferred for these products, such as methanol and ethanol, the concentration of these products is so low that it is not possible to detect. On the other hand, as discussed before, it is also expected that

portion of the electrons contributed to the structural, morphological and even compositional changes of the electrodes.
The comparison of Faradaic efficiencies (FE) at different applied potentials in the table below highlights the enhanced performance of the Sn-Bi_2O_3 and Sn-In_2O_3 electrodes in formic acid production compared to the blank Sn electrode and the Sn-on-Sn electrode. The significantly higher FE observed for the metal-oxide drop-casted electrodes reinforces the notion that oxide-derived bimetallic catalysts provide an advantageous approach for CO_2 reduction, due to the reasons discussed in **Section 4.3**.

Table 6 Comparison of Faraday efficiency values for formate production reported in this work using blank Sn, Sn on Sn and metal-oxide- Sn-electrodes

Applied Potential vs. RHE (V)	FE (%) Blank Sn electrode	FE (%) Sn on Sn (1min) electrode	FE (%) Sn-Bi_2O_3 electrode	FE (%) Sn-In_2O_3 electrode
-1	68	44	77	56
-0.9	36	48	56	55

To compare it with literature values in a study oxygen-vacancy rich In_2O_3-nanorods were prepared from $In(OH)_3$ precursor using low temperature annealing atmosphere-assisted method. Catalytic testing of these purely oxide electrodes have reached 91.2% FE at -1.27V vs. RHE in 0.1M $KHCO_3$ electrolyte[26]. In another work $In(OH)_3$ precursor was created using co-precipitation, which was then converted to In-oxide via pyrolysis, this process was also done on carbon black substrate. The catalyst was then transferred onto carbon cloth and directly used as a working electrode for electrochemical carbon-dioxide reduction. With 11.6wt% carbon black combined with the oxide the scientist have reached 87.6% FE for formate in their experiments at -1.2V vs. RHE in 0.5M $KHCO_3$ electrolyte[27]. Lastly, the results discussed in the In-Sn electrodeposited catalysts, where the In-Sn catalyst was fabricated on Cu-foil substrate the formate FE was 78.6%[24]. Dropcasted In-precursor electrodes in this work has performed with only 55.8% FE at -1V vs. RHE applied potential. However, it can be argued that the applied potentials for the catalytic testing in all three cases are higher than the ones applied in this work, hence the chances are higher that the formate production is more favourable in those conditions.
As discussed in the previous section Bi-Sn alloy catalysts reportedly performed with 94% FE at -1.14V vs. RHE and 94.8% at -1V vs. RHE in 0.5M $KHCO_3$ electrolyte[25], [28], while the Bi-oxide drop-casted Sn-plates reached a maximum of 76.8% FE at -1V vs. RHE. Sn-doped Bi-oxide catalysts via solvothermal method were also tested for carbon dioxide reduction in another study. 2.5% Sn-doped catalyst exhibited the highest FE performance for formate with 93.4% at -0.97V vs. RHE in 0.5M $KHCO_3$ electrolyte[29].

Metal-oxide drop-casted electrodes after electrocatalysis

Due to the reducing potentials applied during the electrocatalysis it is expected that the secondary metal-oxides drop-casted on the Sn-plate electrode will undergo some changes. To investigate the electrodes XRD scan was performed on the air-dried electrodes after electrolysis.

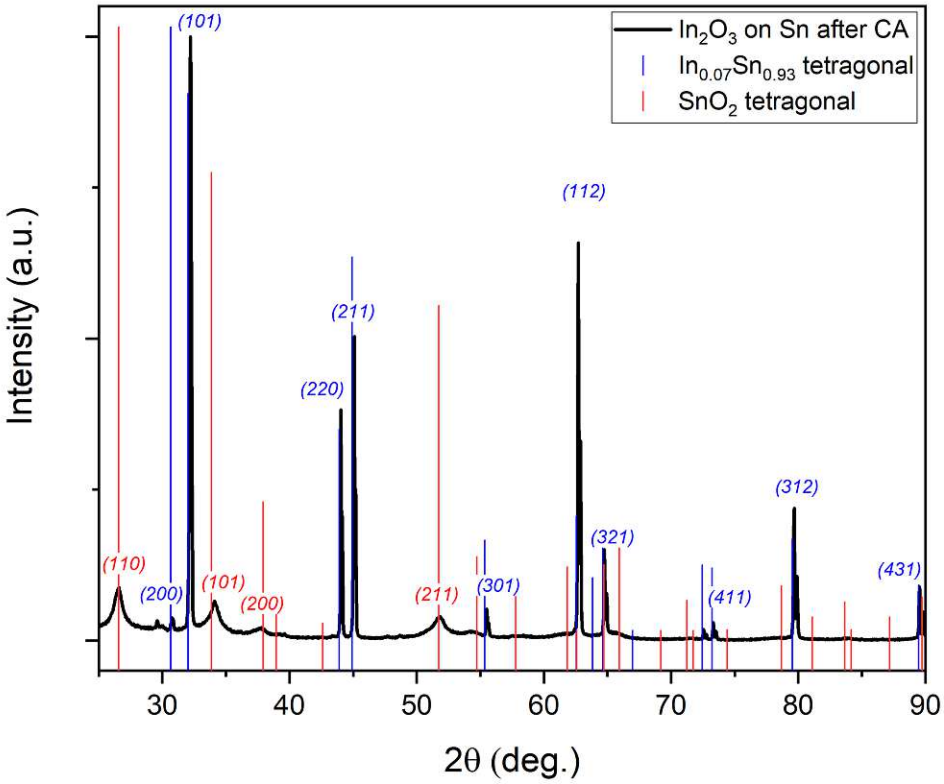

Figure 36 XRD pattern of In-oxide dropcasted Sn-electrode after electrolysis

In the case of the In_2O_3-dropcasted electrodes the same type of surface alloy has formed as in the case of the 55s electrodeposited In-Sn catalyst. Notably, with the in-situ alloying process a decreasing trend with decreasing potentials becomes prominent, while the electrodeposition method offered better performance overall at the lower applied biases. In this sense it would be interesting to investigate whether the process of in-situ alloying offers a way to enhance the stabilization of the preferred key intermediate to form formic acid in this electrocatalytic reaction. Apart from the intermetallic compound weakly defined peaks of Sn(IV)-oxide was also detected on the surface, considering the broadness of the reflex peaks, it is most likely that the volume and amount of the Sn-oxide crystallites are rather small, it is further supported by the fact that lower intensity peaks at higher 2 theta angles are lost in the background of the diffraction pattern.

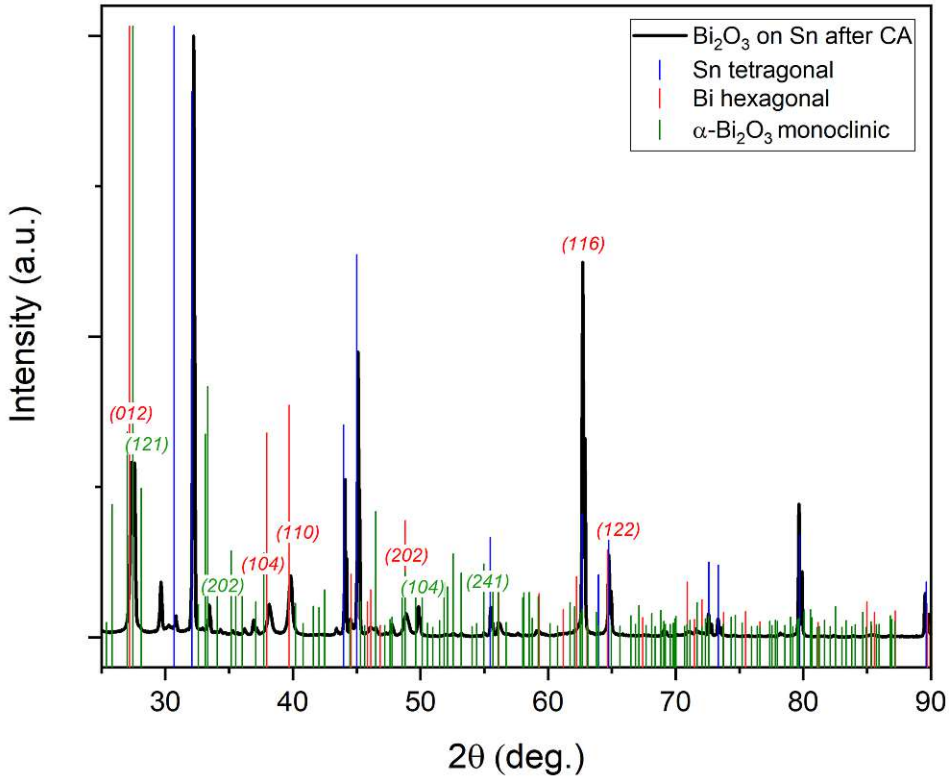

Figure 37 XRD pattern of Bi-oxide dropcasted Sn-electrode after electrolysis

Moving over to the Bi_2O_3 dropcasted electrodes the XRD pattern revealed a separate pure Bi-phase forming during the electrolysis, while also maintaining some of the oxides on the surface. A study suggests, the possibility of the existence of a metastable oxide playing a role in enhanced catalytic activity, when dealing with Sn/SnO_2[16], the possibility of the Bi_2O_3 contributing the same way therefore is a strong hypothesis supported by the higher FE values reached with this type of electrode in comparison to the BiOI electrodeposited Sn-plates, where the post-electrolysis examination revealed that only hexagonal Bi-phase has formed during the in-situ reduction.

6. Conclusions and Outlook

The objective of this work was to fabricate bimetallic catalysts for the efficient conversion of carbon dioxide to formic acid using straightforward electrode production methods. While many works on this exact topic have created interesting and often complicated structures and morphologies to achieve highly efficient formate production, this thesis has focused on targeting novelty while keeping the preparation methods simple. Electrodeposition offers a great opportunity to create pure metallic layers and the method is greatly tuneable in various ways. It has been revealed in this work that a smooth, uniform layer does not offer an advantageous approach towards carbon dioxide reduction, which was also discussed in literature, due to the lack of active sites on the surface[9]. However, assumably the *in-situ* alloying process taking place during the CO_2 reduction experiment increases formic acid production in comparison to the electrodeposited samples, which was observed when a secondary metal-oxide (Bi- and In-oxide) was drop-casted onto the Sn-plates. Alloying can change the electronic structure and Fermi level of the electrode in advantageous ways for the key intermediate(s) to stabilize more effectively. Furthermore, possible morphological and structural changes can promote the creation of more active sites to catalyze formic acid production. This can manifest again in the stabilization of the key intermediate(s), or in enhanced CO_2-adsorption and activation on the surface, due to newly emerging facets and defect sites. XRD scans also confirm that these metal-oxide-Sn electrodes turn into bimetallic alloy upon the in-situ reduction during the electrocatalysis in the case of In-oxide, while Bi-oxide phase still persists even after reduction, but also forms pure metallic Bi-layer on the surface.

While ^{1}H-NMR worked quite well to detect and quantify formate in the liquid phase, it would be necessary to figure out a more suiting method for the detection and quantification of other liquid products such as liquid chromatography. Drawback of this method is volatile products in low concentrations cannot be detected[31]. To target this issue, other quantification methods such as HPLC, GC-MS/FID, or even FTIR could offer a way to build up a better analyzing system. Furthermore it is also concluded in literature that the FE values for formate production tend to moderately fluctuate using Sn-based catalysts and the selectivity and performance is heavily dependent on the chemical structure of Sn and its alloying partners[36].
When the electrolysis time was increased from 1h to 4h in the case of In-deposited and BiOI-deposited Sn-electrodes trace amount of methanol or ethanol were observed as well. The product formation is at a very low rate and therefore the quantification and the proper identification of this product was not possible, however the characteristic triplet peak for both alcohols in the H-NMR spectrum has appeared in some of the electrolysis samples using these catalysts. Due to the fact that the main product during these experiments has proven to be formate this thesis only dedicates this section to discuss the findings, *Section 9 (Figure 36 and 37.)* offers some spectra of these experiments to support the claims. To efficiently produce any of the alcohol products with these bimetallic type catalysts the experiment parameters such as applied voltage, electrolyte, cell design, have to be meticulously tuned, as well as the catalysts architecture.

7. References

[1] Li, C.; Zhou, X.; Zhang, Q.; Xue, Y.; Kuang, Z.; Zhao, H.; Mou, C.-Y.; Chen, H., ChemSusChem, (2022) 15, e202200188.

[2] Wang, Y. Q. Y., Electrocatalysis in balancing the natural carbon cycle, University: Weinheim, Germany (2021). Chapters: 2.4, 3.2.1.1, 16.2.1, 16.2.3

[3] Yang, Z.; Oropeza, F. E.; Zhang, K. H. L., APL Materials, (2020) 8.

[4] Bulushev, D. A.; Ross, J. R. H., ChemSusChem, (2018) 11, 821.

[5] Kim, T. W.; Choi, K.-S., Science, (2014) 343, 990.

[6] Hietala, J.; Vuori, A.; Johnsson, P.; Pollari, I.; Reutemann, W.; Kieczka, H., In Ullmann's Encyclopedia of Industrial Chemistry, ed., p1.

[7] Grasemann, M.; Laurenczy, G., Energy & Environmental Science, (2012) 5, 8171.

[8] Eppinger, J.; Huang, K.-W., ACS Energy Letters, (2017) 2, 188.

[9] Tao, F., Chemical Society Reviews, (2012) 41, 7977.

[10] Wang, M.; Liu, S.; Chen, B.; Tian, F.; Peng, C., ACS Sustainable Chemistry & Engineering, (2022) 10, 5693.

[11] Hori, Y.; Wakebe, H.; Tsukamoto, T.; Koga, O., Electrochimica Acta, (1994) 39, 1833.

[12] Zhang, X.; Guo, S.-X.; Gandionco, K. A.; Bond, A. M.; Zhang, J., Materials Today Advances, (2020) 7, 100074.

[13] Wen, G.; Lee, D. U.; Ren, B.; Hassan, F. M.; Jiang, G.; Cano, Z. P.; Gostick, J.; Croiset, E.; Bai, Z.; Yang, L.; Chen, Z., Advanced Energy Materials, (2018) 8, 1802427.

[14] Liu, L.; Akhoundzadeh, H.; Li, M.; Huang, H., Small Methods, (2023) 7, 2300482.

[15] Zhu, D. D.; Liu, J. L.; Qiao, S. Z., Advanced Materials, (2016) 28, 3423.

[16] Chen, Y.; Kanan, M. W., Journal of the American Chemical Society, (2012) 134, 1986.

[17] Feng, X.; Jiang, K.; Fan, S.; Kanan, M. W., Journal of the American Chemical Society, (2015) 137, 4606.

[18] Zhang, S.; Kang, P.; Meyer, T. J., Journal of the American Chemical Society, (2014) 136, 1734.

[19] Zhang, R.; Lv, W.; Lei, L., Applied Surface Science, (2015) 356, 24.

[20] Cui, C.; Han, J.; Zhu, X.; Liu, X.; Wang, H.; Mei, D.; Ge, Q., Journal of Catalysis, (2016) 343, 257.

[21] Liu, M. F.; Zhang, C.; Wang, J.; Han, X.; Hu, W.; Deng, Y., Chemistry – A European Journal, (2024) 30, e202303711.

[22] Zhao, C.; Wang, J., Chemical Engineering Journal, (2016) 293, 161.

[23] Lv, W.; Zhang, R.; Gao, P.; Lei, L., Journal of Power Sources, (2014) 253, 276.

[24] Dong, W. J.; Yoo, C. J.; Lee, J.-L., ACS Applied Materials & Interfaces, (2017) 9, 43575.

[25] Zheng, H.; Wu, G.; Gao, G.; Wang, X., Chemical Engineering Journal, (2021) 421, 129606.

[26] Cheng, Q.; Huang, M.; Xiao, L.; Mou, S.; Zhao, X.; Xie, Y.; Jiang, G.; Jiang, X.; Dong, F., ACS Catalysis, (2023) 13, 4021.

[27] Mou, K.; Chen, Z.; Yao, S.; Liu, L., Electrochimica Acta, (2018) 289, 65.

[28] Li, Z.; Feng, Y.; Li, Y.; Chen, X.; Li, N.; He, W.; Liu, J., Chemical Engineering Journal, (2022) 428, 130901.

[29] Li, X.; Wu, X.; Li, J.; Huang, J.; Ji, L.; Leng, Z.; Qian, N.; Yang, D.; Zhang, H., Nanoscale, (2021) 13, 19610.

[30] Sun, Z.; Ma, T.; Tao, H.; Fan, Q.; Han, B., Chem, (2017) 3, 560.

[31] Dutta, N.; Bagchi, D.; Chawla, G.; Peter, S. C., ACS Energy Letters, (2024) 9, 323.

[32] Shen, C.; Xu, N.; Guan, R.; Yue, L.; Zhang, W., Ionics, (2021) 27, 3647.

[33] Song, H.; Chen, J.; Sun, B.; Qi, C.; Huang, S.; Yue, K.; Wang, S.; He, J., Ceramics International, (2023) 49, 39342.

[34] Hu, B.; Hu, M.; Guo, Q.; Wang, K.; Wang, X., Applied Catalysis B: Environmental, (2019) 253, 77.

[35] Liu, A.; Gao, M.; Ren, X.; Meng, F.; Yang, Y.; Gao, L.; Yang, Q.; Ma, T., Journal of Materials Chemistry A, (2020) 8, 3541.

[36] Won, D. H.; Choi, C. H.; Chung, J.; Chung, M. W.; Kim, E.-H.; Woo, S. I., ChemSusChem, (2015) 8, 3092.

[37] Conversion of potentials: https://mcauleygroup.net/article/1/

[38] Standard electrode potential values used in these thesis: https://en.wikipedia.org/wiki/Standard_electrode_potential_(data_page)

[39] Mazloomi, K.; Gomes, C., Renewable and Sustainable Energy Reviews, (2012) 16, 3024.

[40] Kim, T.; Devalla, V. S.; Dunfield, S. P.; Palmer, J. R.; Dorr, S.; Kodur, M.; Gupta, A.; Fenning, D. P., Sustainable Energy & Fuels, (2023) 7, 3395.

[41] Rende, K.; Kayan, D. B.; Arslan, L. Ç.; Ergenekon, P., Materials Today Communications, (2023) 35, 105819.

[42] Linganiso, E. C.; Motaung, T. E.; Linganiso, L. Z.; Tetana, Z. N., Materials Letters, (2020) 260, 126883.

[43] Wang, S.; Kou, T.; Baker, S. E.; Duoss, E. B.; Li, Y., Materials Today Nano, (2020) 12, 100096.

[44] Wang, J.; Mao, J.; Zheng, X.; Zhou, Y.; Xu, Q., Applied Surface Science, (2021) 562, 150197.

[45] Xu, C.; Qiu, P.; Li, L.; Chen, H.; Jiang, F.; Wang, X., ACS Applied Materials & Interfaces, (2018) 10, 25321.

8. Acknowledgement

I would like to express my gratitude to Prof. Dominik Eder for giving me the great opportunity to conduct my thesis research in his group. This opportunity has led me gain copious amount of experience on how to carry out a good scientific research and knowledge in the field of material chemistry. His insights and expertise were crucial to the completion of this work which I greatly appreciate.

My sincere thanks also go to Dr. Dogukan Hazar Apaydın, whose guidance and advice were instrumental in the research and writing process. I am grateful to be introduced to the field of electrocatalysis by an amazing and knowledgeable scientist like him. Thanks for always being available to answer my questions (sometimes even silly ones) and listening to concerns sometimes even unrelated to my thesis. Supervising me while becoming a father to a sweet son is not an easy task, but he managed flawlessly. I will always remember the great discussions over coffee breaks, with the best dad jokes that made everybody laugh.

I cannot forget to mention my appreciation for the entire Eder research group. I feel fortunate to have met and worked with such amazing people. It never ceased to impress me how everyone in the group was always glad to provide help and support whenever I approached them with my issues. I am also grateful for all the fun times outside the lab; they are all part of my fond memories.

I want to express my special thanks to Hannah Rabl for sharing her tips and tricks in the lab and sparing the electrochemical instruments and equipment at the cost of her own time planned for conducting her own experiments; to Jakob Blaschke for taking care of the GC maintenance whenever I approached him; and to Stefan Semir Pfaffel for letting me use his amazing sketches for my catch-up reports and my thesis. Most importantly, I want to thank Stefan for being an amazing thesis buddy, working and figuring out the mysterious ways of electrochemistry with you was always joyful. Tea breaks with you, while cell-purging was running, became an essential morning routine that I always looked forward to.

I would like to thank my sister, who, despite being hundreds of kilometers away, never failed to give me the biggest support in life. Our sisterhood may have started off on the wrong foot as kids, but we grew closer as we got older. Aside from the support you have provided me throughout my life, you will always be a significant role model for me. I hope one day to be able to return all the kindness and unconditional love you have given me.

I am also grateful to my dad, who never questioned my ability to start a life alone abroad and provided me with all the means to become a student in Austria. You always wanted the best for me and my sister, and our achievements would never have become a reality without your tireless work and care.

9. Appendix

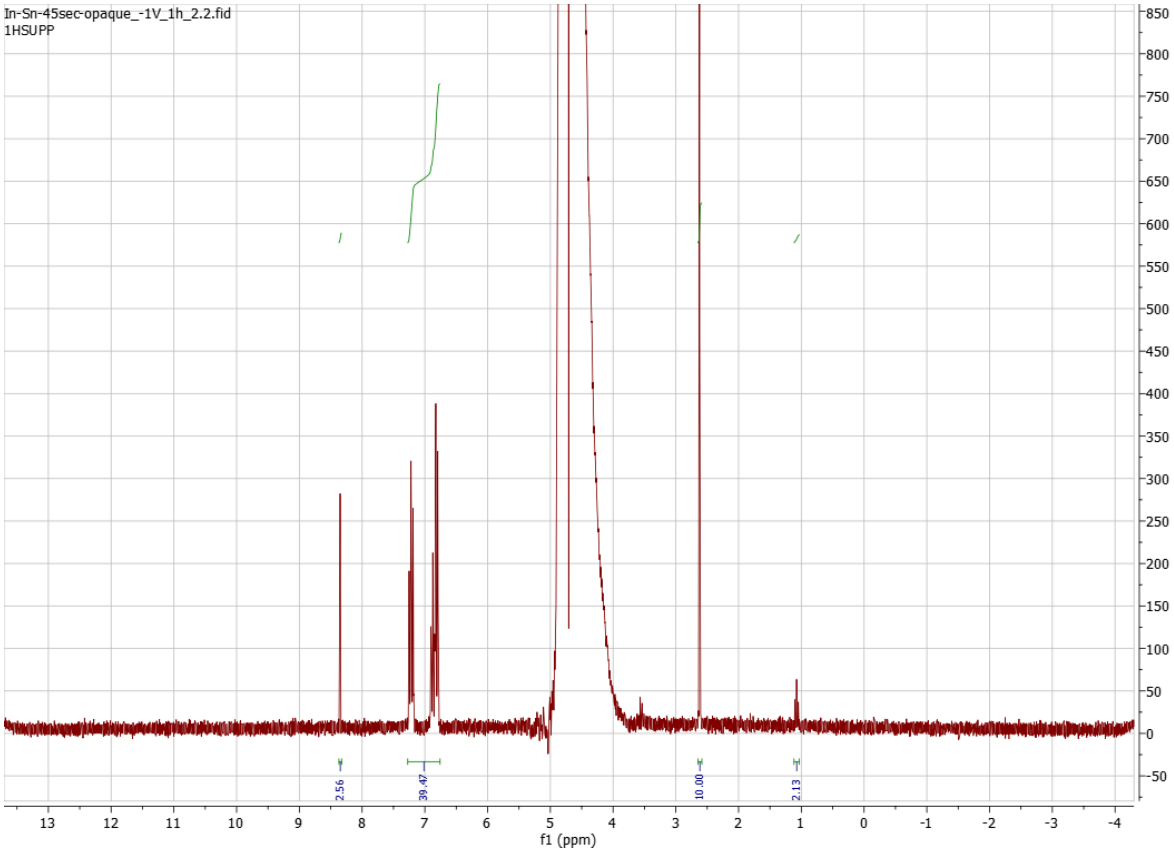

Figure 38 NMR-spectra of catholyte obtained after electrolysis performed with an In-deposited Sn-electrode

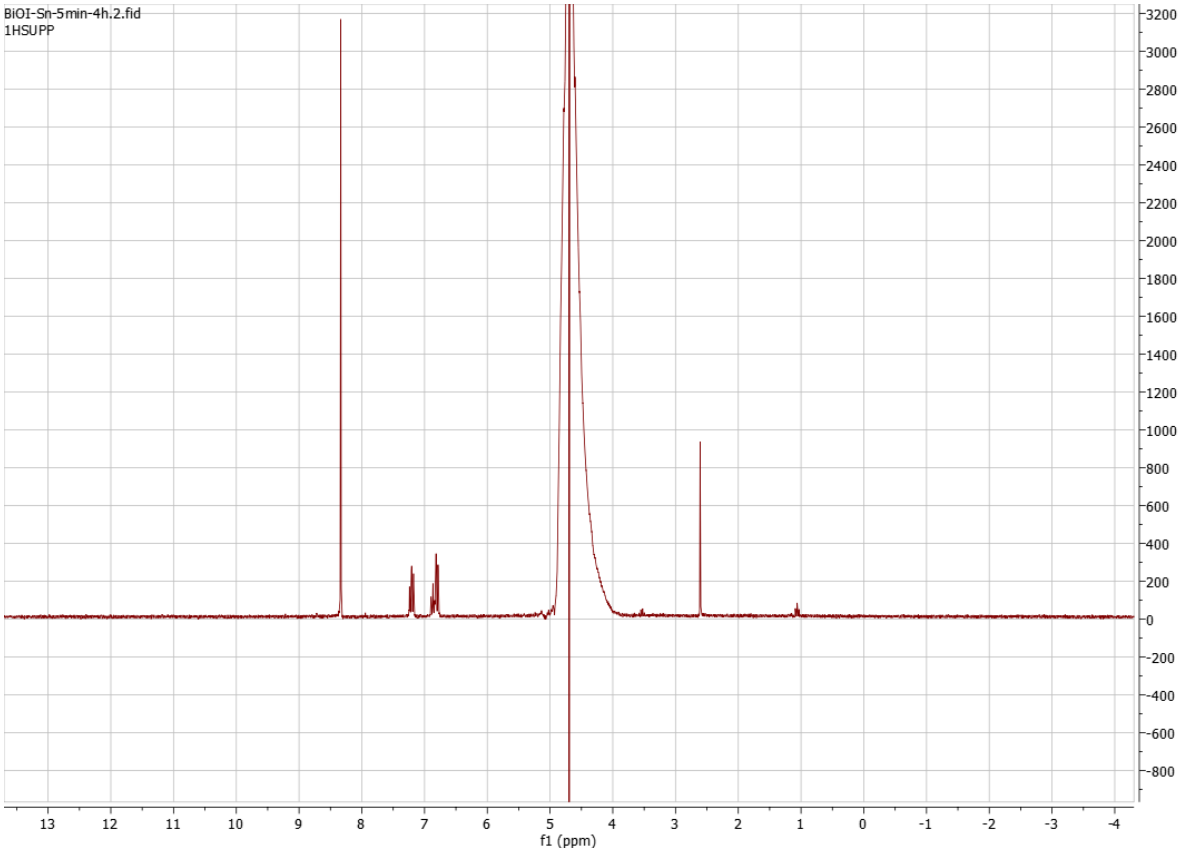

Figure 39 NMR-spectra of an electrode sample obtained after an electrolysis using a BiOI-deposited electrode for initial catalytic performance testing

9.1. List of experiments for electrocatalytic performance testing

Table 7 List of performed catalytic testing experiments

Electrode	Applied Voltage	Duration	Repetition
Blank Sn-plate	-1V	1h	3
Blank Sn-plate	-0.9V	1h	3
Blank Sn-plate	-0.8V	1h	3
Sn-deposited Sn-plate 30s	-1V	1h	1
Sn-deposited Sn-plate 1min	-1V	1h	1
Sn-deposited Sn-plate 2.5min	-1V	1h	1
Sn-deposited Sn-plate 5min	-1V	1h	1
Sn-deposited Sn-plate 1min	-1V	1h	3
Sn-deposited Sn-plate 1min	-0.9V	1h	3
Sn-deposited Sn-plate 1min	-0.8V	1h	3
Sn-deposited Sn-plate 1.5min	-1V	1h	3

Sn-deposited Sn-plate 1.5min	-0.9V	1h	3
Sn-deposited Sn-plate 1.5min	-0.8V	1h	3
In-deposited Sn-plate 30s	-1V	1h	1
In-deposited Sn-plate 45s	-1V	1h	1
In-deposited Sn-plate 1min	-1V	1h	1
In-deposited Sn-plate 1.25min	-1V	1h	1
In-deposited Sn-plate 45s clear	-1V	1h	1
In-deposited Sn-plate 45s clear	-0.9V	1h	1
In-deposited Sn-plate 45s clear	-0.8V	1h	1
In-deposited Sn-plate 45s opaque	-1V	1h	3
In-deposited Sn-plate 45s opaque	-0.9V	1h	3
In-deposited Sn-plate 45s opaque	-0.8V	1h	3
In-deposited Sn-plate 55s opaque	-1V	1h	3
In-deposited Sn-plate 55s opaque	-0.9V	1h	3
In-deposited Sn-plate 55s opaque	-0.8V	1h	3
BiOI-deposited Sn-plate 1min	-1V	1h	1
BiOI-deposited Sn-plate 2min	-1V	1h	1
BiOI-deposited Sn-plate 3min	-1V	1h	1
BiOI-deposited Sn-plate 4min	-1V	1h	1
BiOI-deposited Sn-plate 5min	-1V	1h	1
BiOI-deposited Sn-plate 6min	-1V	1h	1
BiOI-deposited Sn-plate 7min	-1V	1h	1
BiOI-deposited Sn-plate 8min	-1V	1h	1
BiOI-deposited Sn-plate 2min	-1V	1h	3
BiOI-deposited Sn-plate 2min	-0.9V	1h	3
BiOI-deposited Sn-plate 2min	-0.8V	1h	3
BiOI-deposited Sn-plate 3min	-1V	1h	3
BiOI-deposited Sn-plate 3min	-0.9V	1h	3
BiOI-deposited Sn-plate 3min	-0.8V	1h	3
Bi_2O_3-dropcasted Sn-plate	-1V	1h	3

Bi_2O_3-dropcasted Sn-plate	-0.9V	1h	3
Bi_2O_3-dropcasted Sn-plate	-0.8V	1h	3
In_2O_3-dropcasted Sn-plate	-1V	1h	3
In_2O_3-dropcasted Sn-plate	-0.9V	1h	3
In_2O_3-dropcasted Sn-plate	-0.8V	1h	3

9.2. 9.2 List of abbreviations

FE- Faradaic efficiency
WE- Working electrode
CE-Counter electrode
RE- Reference electrode
CV- Cyclic voltammetry
LSV- Linear sweep voltammetry
XRD- X-ray diffraction
CO2RR- Carbon dioxide reduction reaction
HER- Hydrogen evolution reaction
RHE- Reverse hydrogen electrode
NHE- Normal hydrogen electrode
SHE- Standard hydrogen electrode
DI (water)- Deionized water

9.3. 9.3 List of Tables

9.4. 9.4 List of figures